REVIEW

Influence of Cirrus Clouds on Weather and Climate Processes: A Global Perspective

KUO-NAN LIOU

Dept. of Meteorology, University of Utah, Salt Lake City, UT 84112

(Manuscript received 28 January 1985, in final form 16 December 1985)

ABSTRACT

Current understanding and knowledge of the composition and structure of cirrus clouds are reviewed and documented in this paper. In addition, the radiative properties of cirrus clouds as they relate to weather and climate processes are described in detail. To place the relevance and importance of cirrus composition, structure and radiative properties into a global perspective, we present pertinent results derived from simulation experiments utilizing models with varying degrees of complexity, which have been carried out for the investigation of the influence of cirrus clouds on the thermodynamics and dynamics of the atmosphere. In light of these reviews, suggestions are outlined for cirrus–radiation research activities aimed toward the development and improvement of weather and climate models for a physical understanding of cause and effect relationships and for prediction purposes.

CONTENTS

1. Introduction

Cirrus clouds, which regularly cover about 20% of the globe, have been identified as one of the major unsolved components in weather and climate research (Bretherton and Suomi, 1983). Because of high locations in the earth's atmosphere, their detailed microphysical compositions have only recently been studied through the availability of high flying aircraft equipped with sophisticated instrumentation and remote sensing by means of lidar. However, convincing mechanisms as to the formation and dissipation of cirrus as functions of various temporal and spatial scales have not been available either from the thermodynamic or dynamic viewpoint.

Unlike water clouds, high level cirrus, which contain a significant amount of large, nonspherical ice crystals having low concentrations, are normally optically thin and nonblack. It has been recognized physically and numerically that the influence of optically thin and nonblack cirrus on the radiation field of the earth–atmosphere system, and hence on weather and climate components, depends on both the solar and thermal IR radiative properties which, in turn, are modulated by their compositions and physical locations in the atmosphere. The degree and extent of the so-called greenhouse-versus-albedo effects involving cirrus will lead to significant atmospheric differential cooling and heating in vertical as well as horizontal scales. These effects, along with cloud–radiation feedbacks, are recognized to be dominant modes in climatic perturbation processes and appear to have a profound influence on synoptic and global weather systems, at least in time scales longer than three days. In this review paper, we wish to document our current knowledge and understanding of the physical composition and dynamic structure of cirrus and their radiative properties in relation to weather and climate processes and in the context of a global perspective.

In section 2, we present a global view of cirrus clouds from a series of satellite IR cloud pictures. Next, the composition and structure of cirrus clouds derived from in situ observations and remote sensing are described in detail in section 3, where we also introduce the available cirrus cloud climatology. Radiative properties

of cirrus clouds including aspects of light scattering, radiative transfer and broadband flux observations are then defined in section 4. In particular, solar heating and thermal IR cooling profiles in cirrus cloudy atmospheres, along with the definition of the cirrus IR emissivity, are physically discussed. In section 5, numerical experiments that have been performed for the investigation of the effects of cirrus clouds on the thermal and dynamic structure of the earth–atmosphere system utilizing one-dimensional, two-dimensional and general circulation models are reviewed. In light of numerical experiments which have been carried out in past years, primarily for climatic perturbation studies, prospective research activities aimed at a hopeful solution to the intricate problems of cloud–radiation interactions and feedbacks in weather and climate systems are suggested in the summary section.

2. A global view of cirrus from satellites

It has been recognized that cirrus clouds are global in nature and are relatively stable and long-lived, residing as they do in the upper troposphere and lower stratosphere where they are mostly associated with large-scale weather disturbances. Several attempts have been made to identify cirrus clouds from satellite cloud pictures and correlate their activities with the general circulation of the atmosphere (Erickson, 1974; Doswell and Schaefer, 1976; Fraedrich et al., 1976; Wexler and Skellman, 1979). In this section, we wish to describe the formation and dissipation of cirrus clouds on a global scale, based on GOES IR pictures, to place their relevance and importance in weather and climate systems into proper perspective.

Depicted in Fig. 1 for this demonstration is a full disc IR picture at 2345 GMT 23 February 1984. To identify cirrus cloud cover, normal IR grey scales are used, i.e., warmer areas are darker and cooler areas are lighter. Since temperature normally decreases with height in the troposphere, the whitest areas are assumed to be high clouds. The facts that this is a Northern Hemisphere late winter situation, that the polar regions are generally outside the picture, and that the 2345 GMT picture is daytime minimize the chances that the white areas may be associated with cold surface temperatures.

It is quite clear that cirrus is indeed global in nature, being present in all latitudes and without respect to

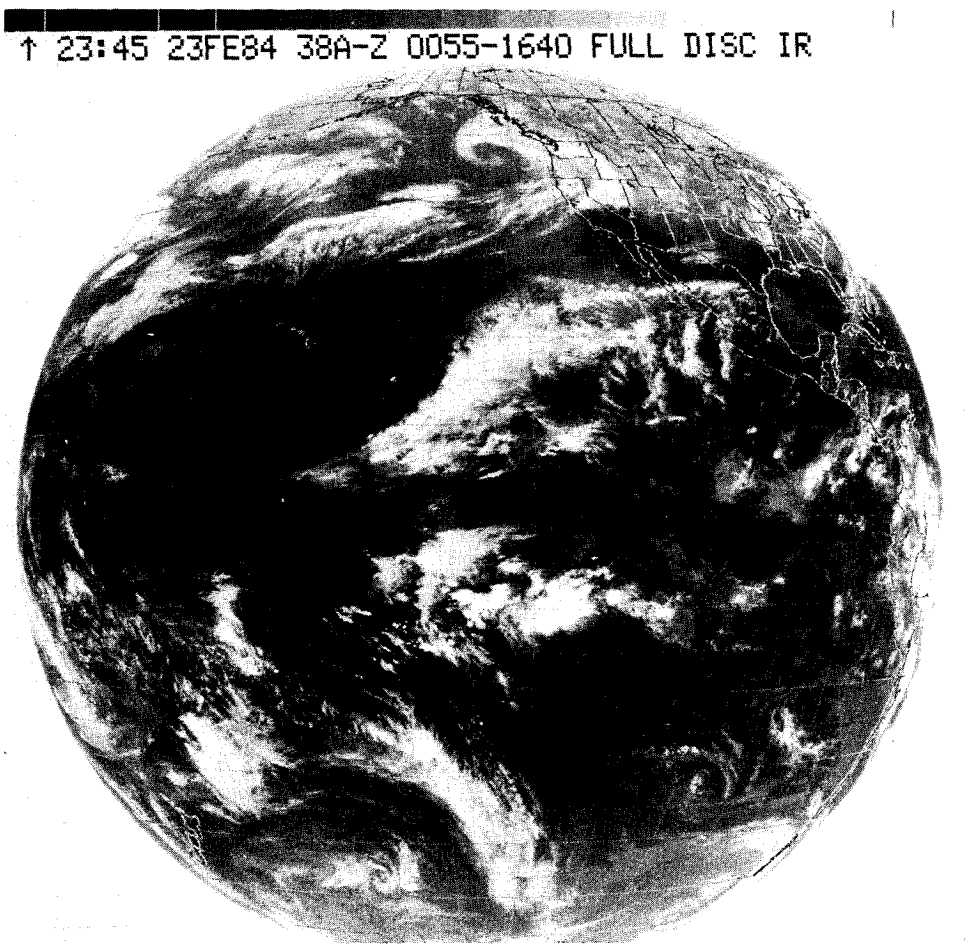

FIG. 1. Full disc IR picture at 2345 GMT 23 February 1984.

land or sea or season of the year. Moreover, it is noted that these clouds, as revealed from subsequent IR pictures, are undergoing changes, sometimes significant, in area coverage, thickness, texture and position. In order to spotlight these changes, the principal cirriform cloud systems presented in Fig. 1 will be described. The most striking cirriform cloud feature is the large spiral-comma-shaped pattern whose center position, estimated by following the spiral cloud counterclockwise and inward to regions of greater curvature, is approximately 800 km west of the Washington coastline. The system is associated with a major surface cyclone located just to the northeast of the cloud center. Lower clouds and precipitation associated with the large-scale rising motion exist under much of this high-cloud canopy. This cloud system runs parallel to and just slightly south of the polar jetstream to 160°W and to the subtropical jet upstream of this point.

To the north of this cloud band over the northernmost areas of the Pacific, another bright cirriform area is associated with a complex of three surface lows and associated frontal systems. Further to the west, the leading edge of a large cirriform cloud mass is moving into the picture, representing a major developing storm off the coast of Japan. Moving southward from the midlatitudes of the Northern Hemisphere, perhaps the most impressive area of cirriform cloudiness in the entire photo is seen over the Pacific Ocean between Hawaii and Mexico. This pattern is associated with a huge, although rather weak trough aloft which is linked with the subtropical jetstream that curves southward near 35°N, 160°W and loops down to near the equator before turning northeastward. The brightness of the cirriform clouds, coupled with light grey areas (middle clouds) below, hints strongly of an active zone of weather activity, although further east, broken, largely transverse bands of cirriform clouds are spreading eastward into Mexico.

The equatorial area in Fig. 1 is characterized by strong, predominantly diurnal convection over western South America with much production of anvil cirrus and a zone of Intertropical Convergence (ITCZ) that extends, in very broken fashion, across the Pacific at 10°S. The most noticeable area of cirriform cloudiness in the ITCZ is in the central Pacific. Here, a collection of mesoscale and synoptic scale clusters of cumulonimbus, some embedded in areas of middle clouds, is producing the brightest (coldest) cirriform cloudiness in the picture. The area is moving slowly westward, characteristic of many disturbances in the ITCZ, although cirrus outflow indicates the presence of a trough aloft over the area, which may be enhancing the development.

In the Southern Hemisphere, the dominant cirriform cloudiness is associated with the strong cold front that extends north-northwestward from an occluded front anchored in an intense low centered at 57°S, 140°W. Other features of interest in the Southern Hemisphere, which has a late summer circulation that is as intense as the late winter circulation of the Northern Hemisphere, include a low pressure system that has been cut off from the westerlies at 31°S, 104°W, characterized by some spiral shaped cirrus and middle clouds. On the western edge of the picture, a weak cold front with a thin cirrus band approaches New Zealand. Finally, to the north of this front, a band of cirrus stretching north-northwestward from 30°S, 165°E is associated with a surface low at 19°S, 158°E and a shear line aloft.

At this point, we have described the principal cirriform cloud systems at 2345 GMT 23 February 1984; the changes in these systems during the ensuing 48 h will now be briefly noted. The cirriform cloud pattern west of Washington depicted in Fig. 1 changes from the well-defined spiral with the original surface low to a disorganized, blotchy mass of less bright (warmer) clouds during the dissipation–reformation process, and finally to a redevelopment of brighter, more organized masses coming together with the major storm development (48 h later, as shown in Fig. 2).

A hugh cirriform spiral, characteristic of extratropical storms, developed from the large cloud mass in the north Pacific that was associated with three surface low pressure areas (Fig. 2). The thin line of cirrus on the poleward side of the cold frontal band stretched from 47°N, 135°W to 35°N, 154°W. This line is adjacent to the polar jet stream which cuts across the frontal zone near the west coast of central British Columbia. To the north of this intersection of jet stream with frontal zone, the cirrus is less bright than the cirrus to the south of the jet. Another major storm that boasts a huge cirriform frontal band and a spiral center at 43°N, 161°E is also seen in Fig. 2. This is the same storm that was just coming into view from the west in Fig. 1.

The principal equatorial feature in Fig. 2 is the ITCZ near 5°S stretching across the Pacific Ocean. This zone is much better defined than in Fig. 1 because it is composed of at least six synoptic scale areas of bright cumulonimbus cloud clusters which generally move east to west. In the Southern Hemisphere there has been relatively little change in the 48 h period between Figs. 2 and 1 due to the fact that the 500 mb flow pattern was initially a Rex-type blocking situation. Lastly, the cirriform band of cloudiness near 55°S, 175°W in Fig. 2 is associated with a strong, new cold front beginning to sweep northeastward.

In light of the aforementioned description, it is quite evident that the formation, maintenance and dissipation of cirrus clouds are directly associated with large-scale synoptic features and disturbances and in part related to deep-cumulus outflows. While the mechanisms are understood qualitatively, the quantitative basis for their formation and dissipation has not been physically resolved. In addition, the question of the feedback of cirrus formation to the synoptic and deep-cumulus systems through radiative perturbations as a function of temporal and spatial scales and its relevance

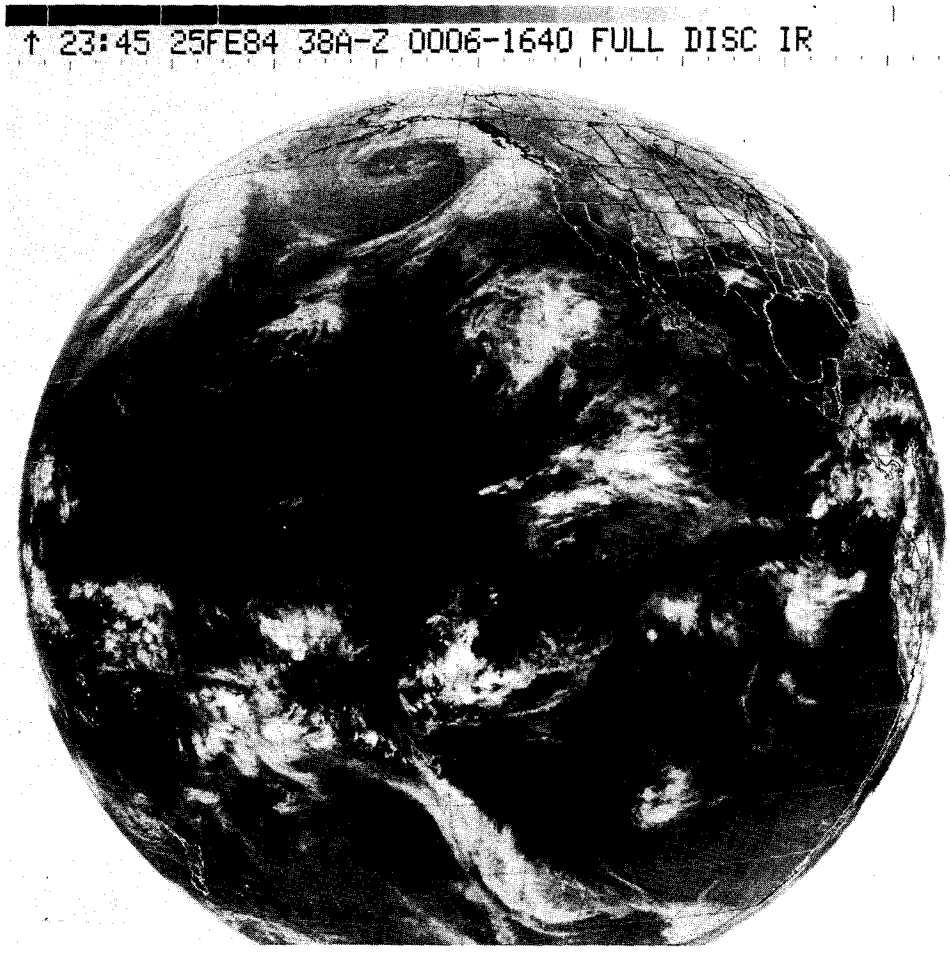

FIG. 2. As in Fig. 1 except for 25 February 1984.

to weather and climate prediction is still open to scientific speculation.

Finally, it should be pointed out that in the preceding discussion, we have completely ignored the problem of thin cirrus. We note that thin cirrus was reported over Alabama in Fig. 1 by ground weather observers. In the IR picture, this cirrus is barely seen as a thin grey streak running north–south through the state. It is clear that this type of cloudiness over data sparse regions such as the ocean would often go unidentified. It is also clear that the identification of thin cirrus by using IR temperature techniques from satellites is extremely difficult, in view of the fact that they are far from blackbodies. Certainly, the physical and dynamic mechanisms for the formation and dissipation of globally distributed thin cirrus and their effects on weather and climate systems are questions unlikely to be resolved without considerable research effort.

3. Composition and structure of cirrus

a. In situ observations

Weickmann (1945, 1947) was the first cloud physicist to undertake the measurement of the composition of cirrus in the atmosphere. Using the technique of direct in-flight samplings by means of oil-covered slides and, subsequently, microphotographs, he showed that cirrus clouds are predominantly composed of columnar crystals. In cirrostratus, crystals have a length of approximately 100 μm and a width of about 40 μm which vary with temperature, duration of supersaturation, and concentration. The concentration of ice crystals in cirrostratus clouds is about 100–1000 L^{-1}. In cirrocumulus, it was found that ice crystals are in the form of bundles of incompletely built columns. The length of one component of such a bundle is on the average about 200–300 μm with a width of 50–100 μm. According to Weickmann, the water content in cirrus clouds is of the order of 0.01 g m^{-3} (see also Aufm Kampe and Weickmann, 1957).

On the basis of snowflake replicas collected throughout the world, Schaefer (1951) reported that cirrus clouds result from spontaneous nucleation and that common crystal types in cirrus are the hexagonal plate and column and the irregular or asymmetric crystal. Evidently, there was a lack of investigation of the composition of cirrus clouds during the '50s and '60s. It was not until the early '70s that the study of the mi-

crostructure of cirrus clouds was carried out (Heymsfield and Knollenberg, 1972). For the first time, the optical-array spectrometers designed by Knollenberg (1970) were used to make continuous particle size distribution measurements in cirrus on a routine basis. The average ice crystal concentration for crystals longer than 15 μm in cirrus generating cells was found to be 10–25 L^{-1}. The mean crystal length is 60–1000 μm with an ice water content of 0.15–0.25 g m^{-3}. The predominant particle habits are found to be columns, bullets, rosettes (75%) and plates (25%).

Hobbs et al. (1975) carried out a series of measurements to explore the distribution and mass concentration of ice in cirrus clouds. An airborne optical ice particle counter designed by Turner and Radke (1973) was used to measure the concentration of ice particles, and a continuous particle sampler with a metal foil impactor was employed to collect and replicate the cloud particles. The crystal shapes associated with cirrostratus, cirrocumulus and cirrus were found to be columns, plates and bullets with sizes ranging from about 100 to 1000 μm. It is noted that many crystals with sizes smaller than 100 μm may be missed by the sampling techniques. The ice water content observed was from about 0.006 to 0.3 g m^{-3}. On the basis of their observations, cirrus clouds appear to be generally associated with upper level troughs.

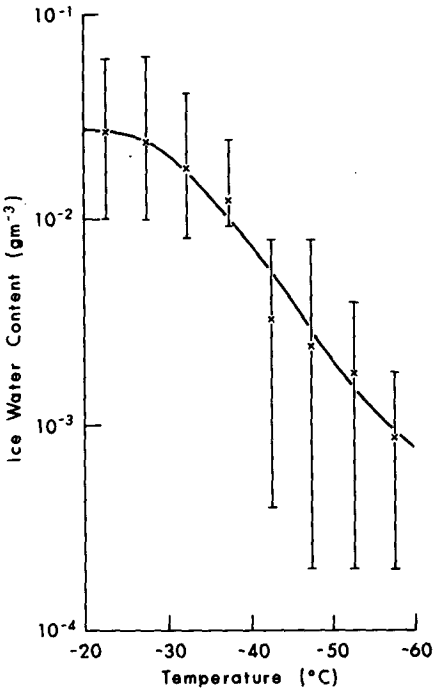

FIG. 4. Ice-water content as a function of temperature. Data from Heymsfield and Platt (1984). The solid curve represents the best fit to the data points.

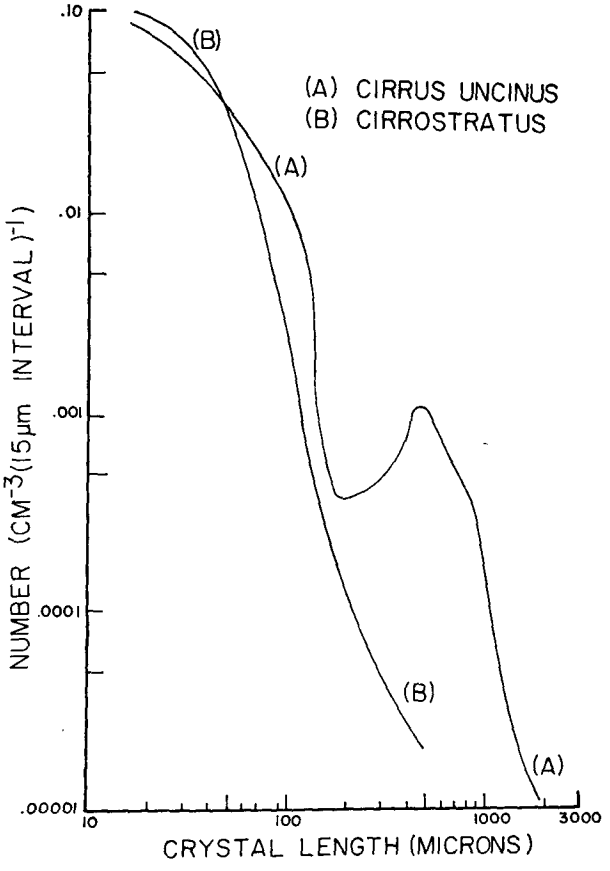

FIG. 3. Ice crystal size distributions for cirrus clouds. (After Heymsfield, 1975a.)

A series of in situ measurements of the microphysical properties of cirrus clouds was also undertaken by Heymsfield (1975a, 1977). In his 1975 paper, he reported observations of ice crystal characteristics for cirrus uncinus and cirrostratus. The predominant ice crystal types found were polycrystalline bullet rosettes, single bullets, banded columns, and plates. The ice water content was found to be less than 0.02 g m^{-3}. Strong evidence for the temperature dependence of particle sizes and concentrations was suggested. Typical particle spectra for these clouds are depicted in Fig. 3. For the cirrus uncinus, we find a biomodal distribution with a second maximum concentration peak at about the 500 μm region. Also, based on this dataset, there are quite a few relatively small crystals (~20–50 μm) existing in cirrus clouds which have not been previously reported. Heymsfield (1977) also presented comprehensive ice crystal data collected from stratiform ice clouds associated with warm frontal overrunning systems, warm frontal occlusions, closed lows aloft and the jet stream. He illustrated that the ice water content and mean length of the ice crystal (via the ice water content) may be correlated with the temperature. Based on this dataset, Heymsfield and Platt (1984) depicted parameterization equations for the ice crystal concentration as a function of maximum dimension and temperature for a 5°C interval from −20° to −60°C. The conclusion derived from their analyses is quite significant from the point of view of radiative transfer computations as

well as the computation of ice content in numerical models. What Heymsfield's measurements (1977) tell us is that temperature is the predominant factor controlling the ice crystal size and the consequence of the ice content. In Fig. 4 we use the data presented in Table 2 of Heymsfield and Platt's paper and fit the observed mean ice content as a function of temperature in the form

$$\ln(\mathrm{IWC}) = -7.6 + 4\exp[-0.2443 \times 10^{-3}(|T| - 20)^{2.455}], \quad |T| > 20. \quad (3.1)$$

Thus, once the temperature for a given layer in the atmosphere is given, the ice content for cirrus clouds may be approximately evaluated if and when the cloud is allowed to form.

In a series of reports, Varley et al. (1980) at the Air Force Geophysics Laboratory presented observations of typical habit and distribution of ice crystals found in relatively thin cirrus clouds. Three instruments were employed in addition to the replicas for the identification of the shape and size of ice crystals in cirrus clouds. These included a scatter probe that was developed for the sizing of spherical water droplets from 20 to 30 μm and Knollenberg's 1-D (26–312 μm, 400–4700 μm) and 2-D (25–800 μm, 200–6400 μm) probes. The predominant crystal form was found to be bullet rosettes with a few plates and columns. The ice water contents for thin cirrus and cirrostratus are, respectively, on the order of 10^{-3} and 10^{-2} g m^{-3}. Since the scatter probe has been recognized to be an unreliable detector for nonspherical ice crystals, it is appropriate to assume that the sizes derived from this instrument did not correspond to the major dimension of the ice particles. Their measurements confirm Heymsfield's observation that a large number of small ice crystals on the order of 20–50 μm exist in cirrus clouds. One interesting fact which I noted from their synoptic analyses was that at least some thin cirrus clouds are directly related to high pressure systems. A summary of the above mentioned aircraft observations is listed in Table 1.

With respect to the aspect ratio (i.e., the ratio of width to length) of ice crystals, Auer and Veal (1970) presented a comprehensive analysis based on available laboratory and field data for various types of ice particles. Heymsfield (1972) made an effort to relate specifically the major and minor axes of ice crystals occurring in cirrus clouds. He derived a number of empirical equations correlating the length (L) and width (d) of bullet (b) and column (c) types for temperatures below about −20°C. These are, respectively, given by (L and d are in units of mm)

$$d_b = \begin{cases} 0.25L_b^{0.79}, & L \leqslant 0.3 \text{ mm} \\ 0.19L_b^{0.53}, & L > 0.3 \text{ mm} \end{cases} \quad (3.2a)$$

$$d_c = \begin{cases} 0.5L_c, & L \leqslant 0.3 \text{ mm} \\ 0.2L_c^{0.41}, & L > 0.3 \text{ mm}. \end{cases} \quad (3.2b)$$

Next, we discuss the orientation problems concerning ice crystals in cirrus clouds. Jayaweera and Mason (1965) studied the behavior of freely falling cylinders in a viscous fluid and found that if the ratio of diameter to length is less than unity, cylinders would fall with

TABLE 1. Aircraft observations of the composition and structure of cirrus clouds.

Investigator	Cloud type	Synoptic condition	Composition
Weickmann (1945, 1949)	cirrostratus, cirrocumulus	—	column, bundle of columns L ~100–300 μm IWC ~0.01 g m^{-3}
Heymsfield and Knollenberg (1972)	cirrus uncinus, cirrostratus, anvil	—	bullet rosette, column (75%), plate (25%) L ~600–1000 μm IWC ~0.15–0.25 g m^{-3}
Hobbs et al. (1975)	cirrus, cirrostratus (~6–7 km)	upper level trough, frontal system	bullet, column, plate L ~100–700 μm IWC ~0.01–0.1 g m^{-3}
Heymsfield (1975)	cirrus uncinus	Temp. ~ −19–−58°C, strong wind shear	bullet rosette, column, plate L ~20–2000 μm IWC ~0.15–3 g m^{-3}
	cirrostratus		L ~20–500 μm IWC ~0.01–0.15 g m^{-3}
Heymsfield (1977)	stratiform ice clouds	Temp. ~ −10–−60°C frontal system jet stream	bullet rosette, column, thick plate L ~300–600 μm IWC ~0.001–1 g m^{-3}
Varley et al. (1978–1980)	thin cirrus, cirrostratus (~8–9 km)	upper level trough high pressure system	bullet rosette, column, plate L ~20–2000 μm IWC ~0.001–0.05 g m^{-3}

their long axes horizontal. Observations by Ono (1969) in clouds indicated that columnar crystals fall with their major axes parallel to the ground, while plates fall with their major axes horizontal. Platt et al. (1978) demonstrated from lidar backscattering measurements that ice crystals in cirrus clouds at approximately −15°C are predominantly plates oriented horizontally. They found that the return signal from ice crystals for vertically pointing laser beams largely retains the polarization state of the incident energy and that for this to occur the plates must be perpendicular to the laser beams.

In view of the aforementioned reviews, we may construct, to the best of our understanding, a general picture of the composition and structure of cirrus clouds as follows.

1) There are several types of cirrus clouds, including thin cirrus and contrails, cirrostratus and cirrus uncinus.

2) Their base heights in the earth's atmosphere vary greatly with respect to seasons and localities, but generally range from 4 to 15 km or so with their cloud base temperatures below about −20°C (see also Appleman, 1961, and further discussion in subsection 3d).

3) Cirrus clouds are composed of predominantly bullets, columns and plates. The fact that halos and sundogs were frequently reported from the aircraft observations reveals that these particles must have a basic hexagonal structure.

4) The ice crystal size distributions vary greatly in cirrus clouds. But for the purpose of radiative transfer calculations, the mean distributions, depicted in Fig. 3 for cirrostratus and cirrus uncinus, are useful.

5) The ice water contents for various types of cirrus clouds may be described by Eq. (3.1) in which they are correlated with the temperature of the cloud.

6) A majority of ice crystals in cirrus clouds seem to be horizontally oriented with their longer axes parallel to the ground.

7) The aspect ratio of bullets and columns in cirrus may be defined by Eq. (3.2).

8) Cirrus (<1 km) and cirrostratus are probably associated with either high pressure systems or upper level troughs. Cirrus uncinus are related to either mesoscale or larger-scale synoptic disturbances.

b. Remote sensing

1) ACTIVE REMOTE SENSING

The utilization of lasers for atmospheric soundings has increased quite rapidly in recent years. The ability to generate very narrow beams and short pulses allows for the atmospheric application of lasers even in daylight. Also, the output of the laser in general contains a high degree of coherence in a well-defined polarization state, permitting additional atmospheric parameters to be measured. The state-of-the-art of laser development has led to the development of lidar systems that use the scattered signal of a laser beam from the atmosphere to identify atmospheric properties by various scattering and absorption processes. One of the applications of lidar systems has been associated with cloud detection. It is noted that with low and middle clouds, many of the attractive advantages of laser beams are substantially degraded due to strong attenuation by multiple scattering and/or absorption of cloud particles.

One of the advances in cloud detection through the use of lidar systems has been the identification of ice and water from the backscattered depolarization signal. Liou and Lahore (1974) and Sassen (1974) demonstrated in theoretical and laboratory settings that nonspherical ice crystals will generate a significant component of cross-polarization from a polarized incident beam whereas spherical water droplets largely retain the polarization state of the incident radiation. Field studies by Sassen (1977), Pal and Carswell (1977), Derr et al. (1977) and Platt et al. (1978) demonstrated quite convincingly the feasibility and applicability of ice–water discrimination from ground-based lidar systems. Sassen (1977) also illustrated the potential of the depolarization technique for the identification of various types of ice crystals and snowflakes. More recently, Spinhirne et al. (1983) employed the backscattered depolarization technique to observe the thermodynamic phase of cloud particles at the cloud top from a lidar system on board a high-flying WB-57F aircraft. Their analysis also demonstrated the potential usage of a space-borne lidar for the detection of thin cirrus. It appears that a satellite-borne lidar system would be quite useful for a precise determination of the top and base heights of cirrus clouds over the globe.

However, in terms of the inference of the composition of cirrus clouds, the success of utilizing lidar systems appears to be quite limited. This is owing to the fact that on one hand, cirrus clouds are composed of a mixture of several types of ice crystals with varying degrees of external complexity and on the other, theoretical understanding of the scattering and polarization of nonspherical and irregular ice crystals is insufficient. While there still appears to be room for improvement in the theoretical analysis and laboratory experiments, it is not entirely clear whether lidar backscattering and polarization techniques could be developed for applications to the inference of the shape and size distributions of ice crystals. In any event, this brief discussion suffices to indicate the limitations of any single remote sensing system.

Nevertheless, lidar systems are ideal tools for monitoring the precise position of cirrus clouds, including, perhaps, invisible cirrus, with respect to their base and top heights and possible layer structure. For that matter, they are also useful for the detection of the base heights of all other clouds. Shown in Fig. 5 is a display of the backscattering returns for a cirrus cloud (courtesy of K. Sassen) from a ruby lidar. The cirrus involved is a thick cloud, but the ruby laser was able to penetrate

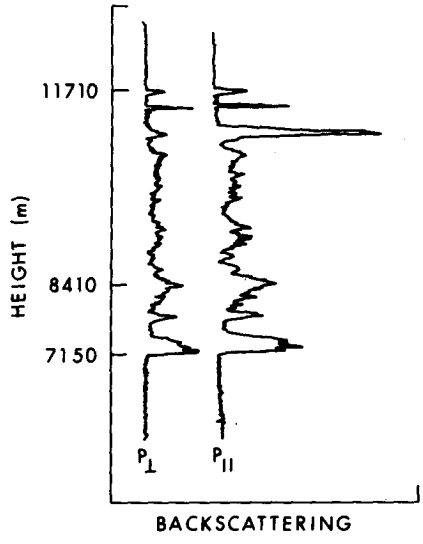

FIG. 5. Backscattering returns of a ruby laser beam from a cirrus cloud (courtesy of K. Sassen). $P_{||}$ and $P_\perp$ denote, respectively, the parallel and perpendicular components with respect to the incident beam.

through the cloud all the way to the cloud top which is located at the tropopause. The backscattered laser beam identifies the cloud base at 7.15 km from both parallel and perpendicular components. The sub-layer structure is clearly illustrated in this graph. The fact that the depolarization ratio, defined as the ratio of the returned parallel power to the perpendicular power, is greater than ~0.3 reveals that ice crystals are predominant in various cloudy layers. The strong backscattering signal (parallel) coupled with a small depolarization ratio suggests that this layer cloud was probably composed of horizontally oriented ice crystals, presumably plates.

In light of the foregoing discussion, it is evident that the detection of cloud positions, especially in the case of cirrus clouds, by means of lidar systems on a routine basis when coupled with conventional cloud observations would enhance the reliability of cirrus cloud climatology from the point of view of the vertical structure. This conclusion is also supported by the fact that it is very difficult to derive reliable and precise information on the cloud position, particularly the base height, from the presently available sounding units on board satellites. Progress in the area of remote sounding of cirrus clouds from satellites will be discussed next.

2) PASSIVE REMOTE SENSING

Orbiting meteorological satellites provide a unique opportunity for observing the earth and the atmosphere globally and on a routine basis. The global cloud pictures from IR emission illustrated in Figs. 1 and 2 serve as good examples of estimating the cloud cover qualitatively based on visual inspection. However, because of the great variability of the optical properties of high cirrus clouds, it is extremely difficult to obtain accurate information about their geographical distribution using conventional visible and IR radiometers. There are two problems encountered in the mapping of clouds. One is concerned with the horizontal cloud cover while the other is associated with the inference of the vertical structure of clouds. As will be discussed below, both cloud parameters are equally important in the radiation field of the earth–atmosphere system and, hence, in weather and climate processes.

In recent years, with the advent of multichannel imagery such as the Advanced Very High Resolution Radiometer (AVHRR) and the great increase in computer power, it has become possible to utilize objective techniques to extract cloud amount as well as some vertical cloud parameters. With the growing interest in developing a cloud climatology, there are now a number of techniques available for extracting cloud cover parameters from the satellite measurements. These techniques can generally be divided into two classes. One uses radiative transfer calculations coupled with a threshold test for the detection of cloudy pixels (e.g., see Rossow et al., 1983), while the other is based on the identification of clusters in multidimensional radiance space formed by one or more channels (e.g., see Coakley and Bretherton, 1982). These techniques normally assume that clouds in the infrared are blackbodies, however.

In a recent paper by Barton (1983), data from two narrow-band channels in the H_2O–CO_2 2.7 μm band on board Nimbus 5 were analyzed to yield the high cloud cover and height information. The advantage to using this absorption band is that because of strong absorption no radiation reflected by the surface or low and middle clouds is detected by the radiometer, except clouds higher than 6 km. Figure 6 depicts the seasonal zonal average distributions of the occurrence of high clouds, presumably cirrus clouds, for a period from December 1972 to February 1975 derived from Barton's study. The region of maximum high cloudiness occurs just north of the equator, except in the Southern Hemisphere summer. The zonal distribution for the winter season has the same feature as the other seasons. However, the maximum and minimum patterns shift 10° to the south. Also, relatively high cloud-free regions are seen to exist near 25°N and 20°S.

Research advances have been made on remote sensing of the vertical structure and amount of clouds, employing sounding radiometers. Smith and Woolf (1976) presented a statistical covariance method for inferring the cloud altitude and amount using the HIRS data. McCleese and Wilson (1976) and Chahine et al. (1977) demonstrated that cloud heights and amounts can be recovered using infrared frequencies in the CO_2 absorption bands. Feddes and Liou (1978) derived the ice and water content of high and middle clouds from parameterization of Nimbus-6 HIRS data using a combination of water vapor and carbon dioxide channels. Liou (1977), in particular, proposed a theoretical retrieval technique to infer the cirrus cloud amount and thickness by means of four radiance measurements

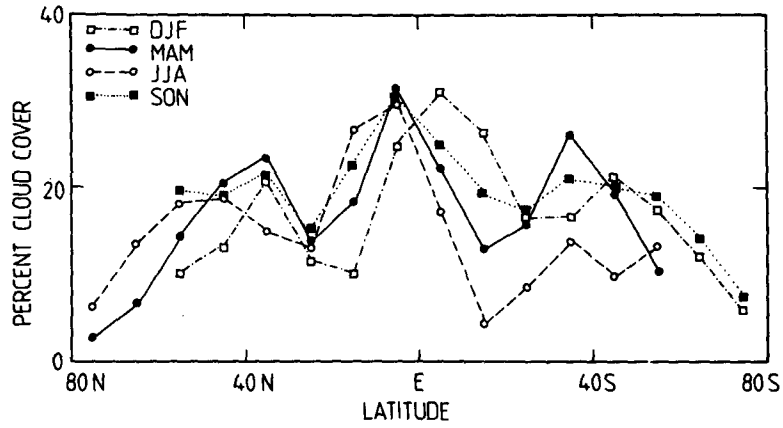

FIG. 6. Seasonal zonal average distributions of the occurrence of high clouds. (After Barton, 1983.)

in the 10 μm window region. More recently, Yeh and Liou (1983) developed a sounding technique based on a parameterization of the infrared radiance transfer for the retrieval of high cloud top height and thickness. Utilizing the concept of adjacent channels in the 15 μm CO_2 band, similar to that discussed by McCleese and Wilson (1976), and combined with the 6.7 μm H_2O band, which has the peak of the weighting function in the vicinity of cirrus clouds, Yeh and Liou demonstrated some success in the derivation of cirrus top height and thickness under overcast conditions. Curran and Wu (1982) developed a technique for remotely determining cloud-top thermodynamic phase and particle size utilizing the measured reflection functions at 0.83, 1.61 and 2.125 μm from multichannel scanning radiometers on Skylab during December 1973. Whether such a technique could be employed for routine observations from a satellite point of view should be explored.

It is conceivable that sounding techniques for the inference of the cirrus top and thickness over the globe in conjunction with the cirrus cloud cover climatology described below may be developed in the future for operational purposes. In conjunction with this, the retrieval program developed by Yeh (1984) appears to shed some light on the possibility of determining cirrus cloud parameters from satellites.

c. *Dynamic formation of cirrus*

In section 2, we pointed out that cirrus cloud systems are normally associated with synoptic and mesoscale disturbances and partly related to deep-cumulus outflows. Our day-to-day experience shows us that cirrus clouds have a fibrous appearance. It is also noted that most extensive cirrus sheets are associated with frontal systems or formed as a widespread anvil cloud remains when the cumulus has dissipated.

Ludlam (1948) first attempted to explain the formation of cirrus uncinus from a thermodynamic point of view. Since ice clouds are generally formed at saturation humidities with respect to water and are therefore at a considerable supersaturation with respect to ice, ice particles grow rapidly on a relative sparsity of effective nuclei and achieve high fall velocities. Because of the wind shear, the typical form of cirrus uncinus appears as a trail of precipitation. Furthermore, Ludlam (1956) described a qualitative mechanism for the continuous generation of ice crystals in localized regions. It was suggested that crystal growth in the ice crystal trails warms the surrounding air due to significant latent heat release. Convective bubbles of the warmed air then rise out of the trails which form fresh clouds after ascending a few hundred meters adjacent to the head of the trail.

Conover (1960) discovered that the most pronounced cirrus bands frequently occur in southwesterly flows adjacent to the jet stream core on the warm side. The cloud region stretches over a narrow area 45–65 km wide and several hundred kilometers long, and it is found that the cirrus bands parallel certain high-level temperature discontinuities. Reuss (1967) found that cirrus bands are formed at the boundary between two air masses of different temperatures and are located just above the layers of strong vertical wind shear. The vertical structure of cirrus clouds was not discussed in these two papers.

The mechanisms for the formation of cirrus uncinus clouds, in connection with their shape and extent, were investigated by Yagi et al. (1968). Using observations by stereophotographs which were analyzed by a trigonometric method, they explained that the movement and elongation of cirrus uncinus were due to the prevailing vertical wind shear at the cloud level. Also, they pointed out that the horizontal component of the comma-shaped cirrus could not be explained without consideration of the temporal and spatial variations of the vertical wind shear at the cloud level. Harimaya (1968) constructed a microphysical model coupled with assumed horizontal winds to quantitatively compute

the shape of cirrus uncinus. Based on numerical computations, he concluded that the shape of cirrus uncinus depended on the mass of ice particles (but not so much on the ice crystal shape) and the vertical wind shear. Although his model did not include an interactive dynamic formation, it was, nevertheless, a first modeling attempt for cirrus clouds. Yagi (1969) further examined the detailed synoptic conditions at the cirrus cloud level, using available radiosonde data and stereophotographs. He found that at the top of cirrus clouds there was a layer with a dry adiabatic lapse rate and vertical wind shear and that above the cloud there was a stable layer which prevents further growth of the cloud. In the case of cirrus uncinus, the trail was in a stable layer, whereas in the case of spissatus and fiblatus clouds, the lower part was quite unstable. From his analysis, it appears that the static stability in the lower part of the cloud plays a significant role in the shape and extent of cirrus clouds. However, in situ cloud physics and dynamic observations were not available.

Based on comprehensive aircraft measurements of the temperatures, horizontal wind velocities and particle spectra at different altitudes, Heymsfield (1975b,c) suggested several plausible physical mechanisms for the formation of cirrus uncinus clouds. For cirrus uncinus oriented perpendicular to the direction of the winds, there appears to be a layer of lifting along which convective cells develop. For isolated cirrus uncinus, there seems to exist a stable layer below the cirrus head region where wave motions generate disturbances from which convection occurs. In addition, Heymsfield argued that there are two different mechanisms for the maintenance of "long-lasting" cirrus uncinus clouds (on the order of several hours). One of these is the local cooling in the trail of the cloud due to evaporation of ice crystals. Also, due to the convergence with positive wind shear and divergence with negative wind shear, which is associated with the downdraft of an existing generating cell, new cells may be produced. A conceptual model of the cirrus uncinus cloud is depicted in Fig. 7 for reference purposes.

It is quite evident in light of the foregoing discussions that the activities of cirrus clouds are of subgrid scale in large-scale numerical models in terms of the horizontal extent as well as the vertical thickness. Consequently, their formation and dissipation will need to be parameterized in numerical models.

In terms of modeling, Starr (1984) recently designed a two-dimensional model specifically for the simulation of the evolution of cirrus clouds. Parameterizations of the vertical velocity of ice crystals, sublimation and evaporation between ice and vapor were carried out. In addition, the eddy terms were expressed in terms of the large-scale diffusion. Depicted in Fig. 8 are contour maps of the ice–water mixing ratio field during a simulation of thin cirrus cloud layers from their model. The maximum ice–water contents shown in these graphs are on the order of 10^{-3} g m^{-3}, close to those observed by Heymsfield and Varley sited previously. His simulation results are quite encouraging in view of the fact that many physical and dynamic simplifications were utilized in the model development. Starr's model was structured with a very fine spatial scale (on the order of 1 km) and the cloud cover was not specifically computed in the model. The manner in which some of the ideas expressed in his work could be utilized in connection with the cirrus cloud formation in general circulation models requires in depth study.

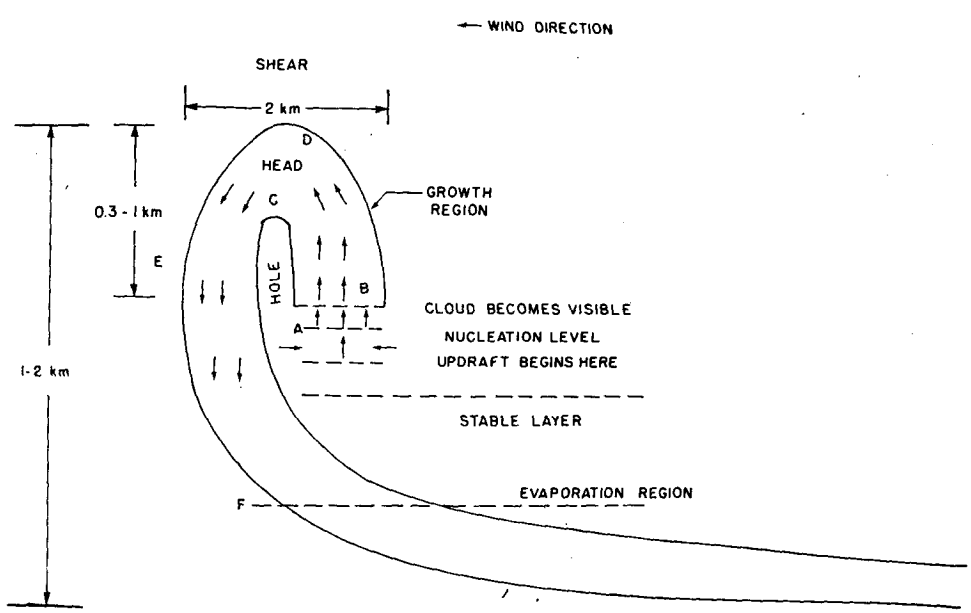

FIG. 7. A conceptual model for the cirrus uncinus cloud. (After Heymsfield, 1975b.)

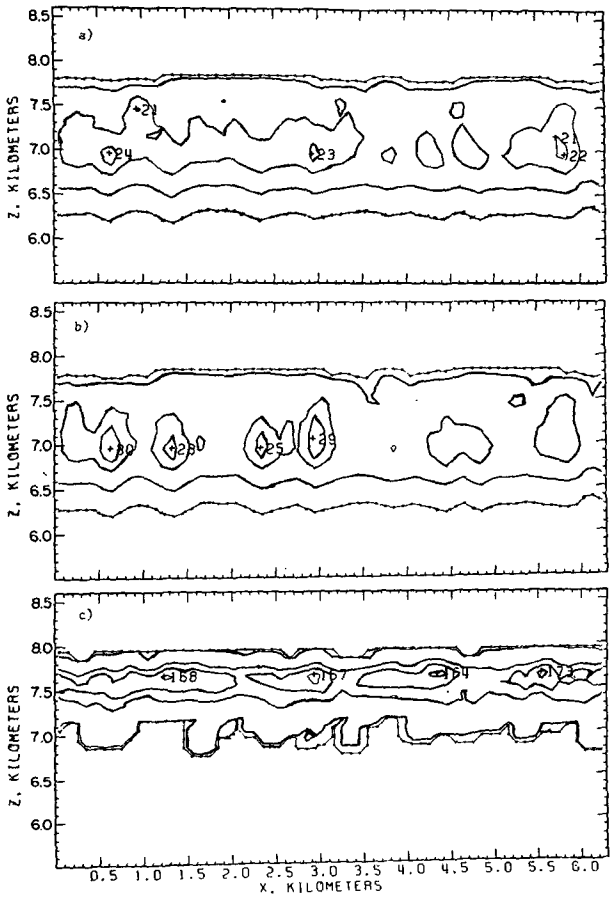

FIG. 8. Contour plots of cloud water mixing ratio at time $t = 30$ min during simulations of (a) cirrus at night, (b) cirrus at midday, and (c) a liquid phase cloud layer at night. Contour levels correspond to $l = 10^{-3}$ (*), 1, 10 and 20 $\mu g\ g^{-1}$ on (a) and (b), and $l = 10^{-3}$ (*), 1, 50, 100 and 150 $\mu g\ g^{-1}$ on (c). (After Starr, 1984.)

To the best of my knowledge, no specific effort has been made to incorporate a physically based cirrus cloud formation scheme into a GCM. However, Sundqvist (1978, 1981) proposed a numerical model for nonconvective condensation processes, intended for incorporation into GCMs, in which the liquid water content as a prognostic variable was introduced. It appears that some of the parameterization processes for evaporation and condensation could be of use to cirrus cloud applications. In order to gain some physical insight into the parameterization requirements of an interactive cloud formation scheme in large-scale weather and climate models, it seems appropriate to present the basic equations governing the specific humidity q and the mixing ratio of cloud water l. In the absence of ice related processes, these are given by

$$\frac{\partial \rho q}{\partial t} + \nabla \cdot \rho \mathbf{V} q = -\frac{\rho}{L}\eta Q + \frac{\rho}{L}(1-\eta)(E_r + E_c) - \nabla \cdot \rho \overline{\mathbf{V}'q'} \quad (3.3)$$

$$\frac{\partial \rho l}{\partial t} + \nabla \cdot \rho \mathbf{V} l = \frac{\rho}{L}\eta Q - \rho P - \frac{\rho}{L}(1-\eta)E_c - \nabla \cdot \rho \overline{\mathbf{V}'l'}. \quad (3.4)$$

In these equations, ρ denotes the density which is needed for the height coordinate, $\mathbf{V}$ the vector velocity, L the latent heat, η the cloud cover, Q the heating rate due to condensation, E_r/L and E_c/L the evaporation rates for rain drops and cloud drops, respectively, P the precipitation generation rate, and $\overline{\mathbf{V}'q'}$ and $\overline{\mathbf{V}'l'}$ the eddy fluxes for the specific humidity and the mixing ratio of cloud water, respectively.

In Sundqvist's pioneering work, the last term in Eq. (3.3) was neglected and the vertical eddy for cloud water was expressed in terms of its average terminal velocity. Also, the large-scale wind field was prescribed in the model using GCM results. The precipitation rate was parameterized in terms of the cloud water which followed the ideas presented by Kessler (1969) and Ogura and Takahashi (1971) for the modeling of mesoscale convective clouds. Moreover, the evaporation rate for rain drops was assumed to be proportional to the square root of the precipitation rate for cloud particles, while the evaporation rate for cloud drops was neglected. Finally, it is noted that Sundqvist did not include an interactive radiation scheme in the thermodynamic equation and assumed a critical relative humidity of 80% to compute the cloud cover. The spatial and temporal distribution of radiative heating and cooling rates will affect the humidity and cloud fields indirectly via the large-scale wind field. For applications to cirrus cloud formation, the terms involving Q, E_r/L, E_c/L and P should be changed and expressed for ice crystal conditions. Processes associated with deposition, sublimation, melting and freezing need to be parameterized in terms of the specific humidity and ice content mixing ratio along with other relevant large-scale variables. The coupling of the cirrus–moisture model with appropriate dynamic settings for cirrus cloud formation is certainly a research area of considerable challenge.

The success of forming cirrus clouds in weather and climate models based on physical principles critically depends on the availability of cloud cover, cloud height, cloud liquid water content and cloud particle data over time and spatial scales compatible with the models. With the increasing availability of global cloud data, for example, from the International Satellite Cloud Climatology Project (ISCCP) and the additional cloud physics and radiation data for cirrus to be obtained from the First ISCCP Regional Experiment (FIRE), we envision the opportunity for a quantum advance in our knowledge and understanding of the dynamic formation of clouds in general, and cirrus in particular, in the context of weather and climate models during the next five years or so.

d. Cirrus cloud climatology

As will be discussed in section 5, clouds may be considered to be the most important parameter controlling the heat budget of the earth–atmosphere system and, hence, its climate. Reliable and detailed cloud information on a global scale is therefore required for the construction of weather and climate models and for the understanding of weather and climate processes. In recognition of the relevance and significance of cloud climatology data to climate problems, the International Satellite Cloud Climatology Project has been established (Schiffer and Rossow, 1983) to provide a five-year global cloud cover climatology from satellite observations, commencing in 1984. Undoubtedly, this project will eventually produce a comprehensive cloud (including cirrus) cover climatology for weather and climate research.

However, the most widely used cloud climatology at present is that developed by London (1957) who compiled available surface cloud observations back in the '30s and '40s. The two primary merits of this climatology are that it provides the zonal distribution of clouds by type and height for the Northern Hemisphere in addition to the distribution of the total cloud cover amount. Clouds were divided into six types which include high clouds (Ci, Cs), middle clouds (As, Ac), low clouds (St, Sc), cumulus, cumulonimbus and nimbostratus. In Fig. 9 the cloud base heights for these six types as functions of latitude are depicted along with their thicknesses and mean annual cloud cover. It is noted that cirrus base heights vary with latitude but their thicknesses are fixed at 1.7 km. It is fortunate that we have London's cloud data for climate studies. However, it is unfortunate that these are the only complete cloud data that are available for use by the scientific community at this time. We also note that Sasamori et al. (1972) gave the fractional cloud cover including cirrus for the Southern Hemisphere.

Collections of cirrus cloud climatologies over specific regions were described by Appleman (1961) in a WMO report. Data include the frequency of occurrence, cloud base heights and thicknesses obtained from the International Cloud Year (ICY) of 1896–97 and reported over Great Britain, the United States, Canada and Western Europe in the '50s. The cirrus heights vary with latitude and season and are comparable to those presented by London. The reported mean thickness of cirrus cloud layers is between about 1–2 km. In London's data, the cirrus thickness is set to be 1.7 km regardless of the latitude and season. The data described and analyzed by Appleman are largely limited over land areas and no attempt was made to derive a global cirrus distribution.

Recently, Woodbury and McCormick (1983) reported the spatial extent and frequency of cirrus clouds analyzed from SAGE (Stratospheric Aerosol and Gas Experiment) extinction data over a 15 month period. The SAGE experiment utilizes the solar occultation technique. The analysis separates cirrus cloud observations into cirrus and thin cirrus based on the observed extinction values from the satellite experiment. SAGE cirrus results were then compared with data presented by Hahn et al. (1982) based on surface observations. Comparisons showed significant differences between two independent datasets. In view of the fact that the surface observations generally underestimate cirrus cloud cover and that SAGE cirrus results require ap-

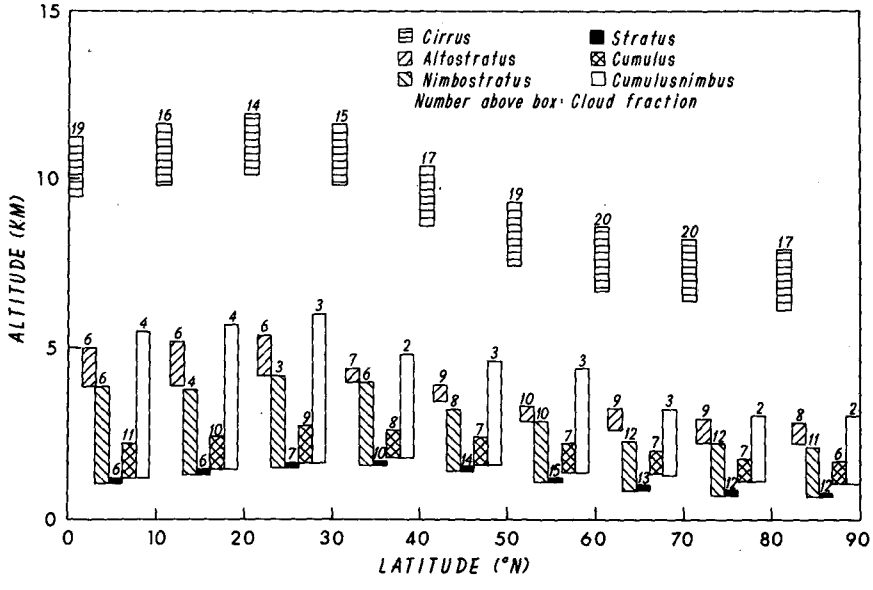

FIG. 9. Zonally averaged climatology of cloud type, cover and thickness, including cirrus, for the Northern Hemisphere.

propriate validations, it is not surprising to find these differences. The cirrus results derived from SAGE are quite interesting and significant, especially for thin cirrus clouds which are frequently missed by surface observations. Also, as pointed out in subsection 3b,2, thin cirrus clouds are extremely difficult to detect from the satellite sounding units currently available. Woodbury and McCormick (1985) extended their analysis to cover the time period from February 1979 to November 1981 and to provide not only the zonally averaged cirrus cloud cover but also the cirrus global distribution. It seems that SAGE data should be carefully analyzed with respect to the frequency of occurrence and position of thin cirrus clouds so as to compliment other cloud climatology efforts.

Although evidence for changes in global average cloudiness does not exist at present because of the lack of proper cloud climatology data, there may exist evidence that more localized cloudiness has increased. Machta and Carpenter (1971) reported on secular increases in the amount of high cloud cover in the absence of low or middle clouds at a number of stations in the United States between 1948 and 1970. It has been suggested (Machta and Carpenter, 1971; Changnon, 1981) that there may be a link between this increase in cloudiness and the expansion of jet aircraft flights in the upper troposphere and lower stratosphere in the latitude range between 30° and 65°N. While it is not the prime objective of this review to speculate on the possible increase in cirrus cloudiness, if this link does exist, however, such an increase may have serious implications for the radiation balance of the earth–atmosphere system and a consequent impact on the planet's climate.

4. Radiative properties of cirrus clouds

To begin the discussion on the radiative properties of cirrus clouds, we shall first describe the optical properties of ice. The index of refraction for ice generally varies in two directions for extraordinary and ordinary waves. However, for all practical purposes, in atmospheric light-scattering and radiative transfer studies, it suffices to use the index of refraction corresponding to the extraordinary wave.

The real and imaginary parts of the refractive index of ice were comprehensively tabulated by Irvine and Pollack (1968) based on available laboratory measurements prior to that year. Schaaf and Williams (1973) measured the absorptivity and reflectivity of a film of ice at −7°C in the wavenumber range 5000 to 300 cm^{-1} and derived the real and imaginary parts of the refractive index. More recently, Warren (1984) carried out detailed compilations and analyses of the real and imaginary parts of the refractive index of ice at −7°C temperature for wavelengths $\lambda < 167$ μm, which should be valid for use at temperatures between −60° and 0°C. Shown in Fig. 10 are the graphs for these values.

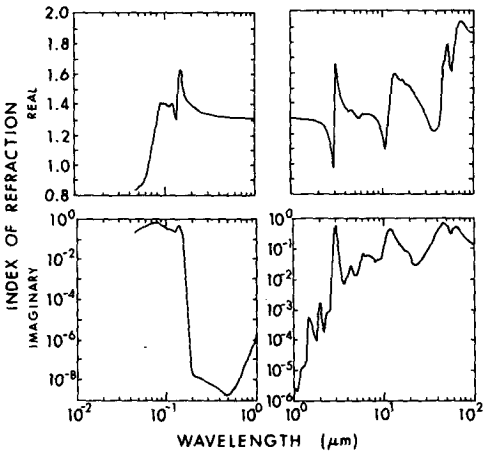

FIG. 10. Real and imaginary parts of the refractive index of ice in solar and thermal infrared wavelengths. (After Warren, 1984 with modifications.)

The real part is seen to vary from 1 to about 1.7 for wavelengths of interest to atmospheric energy studies. The imaginary part which is associated with the absorption coefficient, on the other hand, varies greatly with the wavelength. At 0.9 μm, it is about 10^{-6}, but at 3 μm, a value of 0.75 is seen. It is also noted that ice exhibits relatively strong absorption at about 1.6 μm where water shows a minimum absorption. Because of the rapid variations in the absorption coefficient of ice, care must be taken in the radiative transfer analysis covering the entire solar and thermal infrared spectral regions.

a. Light scattering by ice crystals

In accordance with in situ observations noted in section 3, cirrus clouds are largely composed of nonspherical bullets, columns and plates. Unlike the scattering of light by spherical water droplets, which is governed by the so-called Mie solution, the light scattering and polarization characteristics of these nonspherical ice crystals are largely unknown. In addition, the sizes of these ice crystals range from 10 to 1000 μm, which are comparable to or larger than the typical emission wavelength in the thermal infrared region of the earth–atmosphere system and will therefore affect the transfer of thermal infrared radiation.

Since columnlike crystals are frequently observed, a first approximation to model these particles has been to use circular cylinders for light scattering investigations. Basically, exact far field analytic solutions may be derived and numerically computed from the electromagnetic wave equation in cylindrical coordinates (infinite in the z-direction) for arbitrarily oblique incidence (e.g., see Kerker, 1969; Liou, 1972a). Liou (1972b) made the first attempt to model the single-scattering properties of ice clouds utilizing the scattering

solution for long circular cylinders. Ice cloud models containing preferred and randomly oriented ice cylinders were employed in single-scattering computations. It was found that, when compared with ice spheres, long ice cylinders scattered more light in the side directions at the expense of scattering in both forward and backward directions. In addition, it was also pointed out that the glory and cloud-bow features, which are produced by spherical particles, were either lost or largely reduced and smoothed out due to nonsphericity. Thus, for irregular ice crystals, it should be expected that neither glory nor cloud-bow features should be present. This distinction appears to make possible the differentiation between spherical droplets (or ice particles) and irregular ice crystals by means of active or passive remote sensing. Recently, Stephens (1980a) used the cylindrical scattering solution given by Liou (1972a,b) and performed single-scattering and radiative transfer calculations involving ice clouds.

It is noted that exact scattering solutions for prolate and oblate spheroids from the electromagnetic wave equation were derived and numerically tested (e.g., see Asano and Sato, 1980) and various exact numerical solutions for arbitrary but symmetrical irregular particles were also developed (e.g., see Barber and Yeh, 1975). However, all of these methods have been successful only when size parameters are very small (say less than about 20). Since the sizes of atmospheric hexagonal ice crystals are normally much larger than or at least comparable to the wavelengths in the solar (0.2–4 μm) and thermal infrared (4–50 μm) for applications to the earth and the atmosphere, the geometrical ray tracing method may be utilized to evaluate their scattering characteristics. The geometrical ray tracing method has long been used to understand and to explain the magnificent halos (e.g., see Greenler, 1980).

Computations of angular scattering patterns for hexagonal crystals were first reported by Jacobowitz (1971) assuming infinitely long hexagonal columns. Wendling et al. (1979) and Liou and Coleman (1980) undertook a more comprehensive ray-tracing analysis to evaluate the scattering phase functions for finite hexagonal columns and plates. More recently, Cai and Liou (1982) developed a scattering model involving complete polarization information for arbitrarily oriented hexagonal columns and plates on the basis of ray tracing principles which includes contributions from geometric reflection and refraction and Fraunhofer diffraction.

Shown in Fig. 11 are the scattering phase functions P_{11} for randomly oriented ice columns (120 μm) and plates (20 μm) for an incident wavelength of 0.7 μm (left diagram). Also shown for comparison is the measured scattering phase function derived from a number of scattering experiments for small plates, having sizes of about 5 μm, illuminated by a 0.6328 μm laser beam reported by Sassen and Liou (1979a). The vertical bars in this figure depict the standard deviation of the mea-

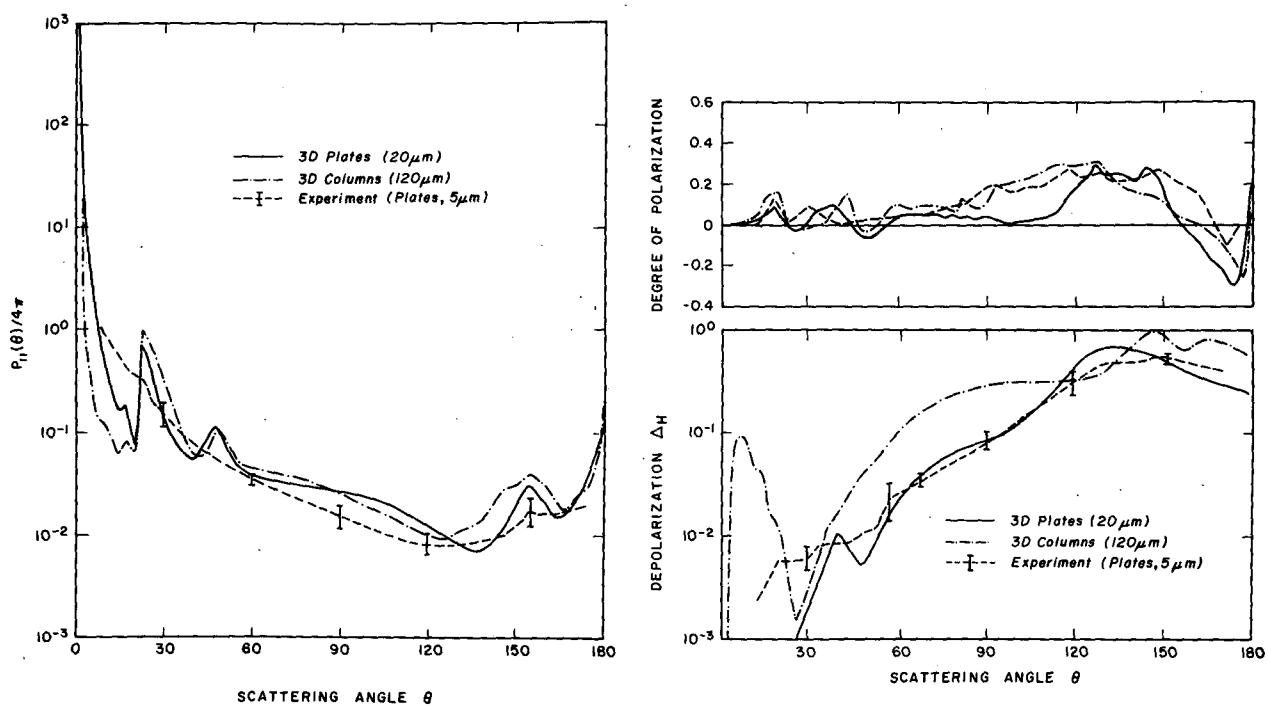

FIG. 11. Comparison of the computed and measured scattering phase functions (left), degree of linear polarization (upper right) and depolarization ratio (lower right) for randomly oriented columns and plates. The modal dimension of the plates observed in the scattering experiments is ~5 μm. (After Cai and Liou, 1982.)

sured data. Large columns generate a larger and broader peak at the 22° halo region and at the 150° scattering angle region. However, the basic features are the same for hexagonal columns and plates. It is noted that the experimental data reveal small maxima at about 22° and 155° scattering angles which are in general agreement with results derived from geometric ray tracing calculations. In addition, illustrated on the right of Fig. 11 are the computed and measured degree of linear polarization and depolarization ratios using a horizontally polarized light for columns and plates. As shown, the computed linear polarization (upper graph) and depolarization ratio (lower graph) for 20 μm size plates closely matches the experimental data for plates having a modal diameter of about 5 μm, presented by Sassen and Liou (1979a,b).

Employing the program developed by Cai and Liou (1982), computations of the single-scattering properties for a number of wavelengths, and columns and plates of various sizes were carried out. Table 2 summarizes the resulting single-scattering parameters including the extinction cross section, single scattering albedo, (i.e., the ratio of scattering to extinction cross sections) and asymmetry factor, denoting the strength of forward scattering by cloud particles. The corresponding wavelength and particle size ($L \equiv$ length, $a \equiv$ radius) along with the refractive indices are also listed in the table. The normalized phase functions as functions of the scattering angle not presented here are also available for cases presented in Table 2. Unfortunately, because of a large amount of computer time required in calculating single scattering parameters and phase functions, we have not been able to obtain these parameters for additional wavelengths and crystal sizes.

The foregoing wavelengths were basically selected for applications to laser transmission and satellite sounding of cirrus clouds from AVHRR. However, for applications to radiative transfer in connection with atmospheric energetics, the single scattering parameters for wavelengths other than those presented here could be extracted by interpolations and extrapolations of the present results and by properly taking into account the slow variation of the refractive index depicted in Fig. 10. Since an exact and efficient Mie scattering program has been available (Wiscombe, 1980), can equivalent ice spheres replace hexagonal ice crystals for single-scattering calculations? In view of the fact that spherical particles do not generate the scattering features described above and that there are no unique rules governing the so-called equivalent spheres with respect to hexagonal crystals, it appears appropriate to state that if intensity patterns are required (e.g., for remote sensing applications) hexagonal crystals should be utilized in the analysis of light scattering and radiative transfer involving cirrus clouds. For flux calculations, the use of equivalent ice spheres to replace hexagonal ice crystals for energetic analyses would require some in-depth investigations. Basically, we need to find the proper manner in which the single-scattering parameters for equivalent ice spheres may be adjusted for net flux and heating rate calculations.

Finally, it should be pointed out that all the single-scattering parameters and phase functions presented in this section are for hexagonal crystals randomly oriented in three-dimensional space. As noted in subsection 3a, large columns, bullets and plates probably will have preferred orientations with their longer axes parallel to the ground. While the mathematical averaging procedure to obtain the scattering phase function for randomly oriented hexagons in two-dimensional space is straightforward (Asano, 1983a), the numerical computations become quite involved and the scattering phase function and extinction and scattering cross sections now depend on the directions of incident and emergent beams.

b. Radiative transfer in cirrus cloud layers

1) SOLAR RADIATION

Solutions to the transfer of solar and thermal infrared radiant intensity through cirrus cloud layers are fun-

TABLE 2. Real and imaginary parts of the refractive index, extinction cross section, single-scattering albedo $\tilde{\omega}_0$ and asymmetry factor g for various wavelengths and crystal dimensions.

L/a (μm)	λ (μm)	m_r	m_i	σ_e (10^{-4} cm^2)	$\tilde{\omega}_0$	g
300/60	0.55	1.310	0.000	5.653*	1.000	0.988
	0.7	1.310	0.000	5.653	1.000	0.987
	1.3	1.296	1.2×10^{-5}	5.623	0.979	0.985
	3.8	1.383	0.007	5.623	0.570	0.982
	10.6	1.097	0.134	5.653	0.531	0.975
	10.8	1.038	0.169	5.653	0.530	0.968
	11.9	1.259	0.409	5.653	0.550	0.967
5/1	0.7	1.310	0.000	0.002	1.000	0.831
2/2.5	0.7	1.310	0.000	0.003	1.000	0.804
30/37.5	10.6	1.097	0.134	0.735	0.561	0.969
8/10	0.6328	1.310	0.000	0.012	1.000	0.895

* The accuracy of σ_e is only up to the third decimal point.

damental to the understanding of solar and IR fluxes, and solar heating and IR cooling rate distributions in cirrus cloudy atmospheres. In this section, we will begin with the discussion of the basic radiative transfer equations with applications to ice clouds. Under the plane-parallel approximation, the transfer of diffuse intensity I_λ in a scattering and absorbing medium, consisting of randomly located spheres or randomly oriented nonspherical particles, for flux applications may be written in the form

$$\mu \frac{dI_\lambda(\tau, \mu)}{d\tau} = I_\lambda(\tau, \mu) - \frac{\tilde{\omega}_\lambda}{2} \int_{-1}^{1} P_\lambda(\mu, \mu') I_\lambda(\tau, \mu') d\mu' - \frac{\tilde{\omega}_\lambda}{4\pi} F_{0\lambda} P_\lambda(\mu, -\mu_0) e^{-\tau/\mu_0} \quad (4.1)$$

where τ denotes the optical depth which is a function of wavelength, $\mu = \cos\theta$, θ the emergent zenith angle, $\mu_0 = \cos\theta_0$, θ_0 the solar zenith angle, $\tilde{\omega}_\lambda = \sigma_{s,\lambda}/\sigma_{e,\lambda}$, the single scattering albedo, σ_s and σ_e the scattering and extinction cross sections, P_λ the normalized scattering phase function, and $F_{0\lambda}$ the incident solar flux. Equation (4.1) is to be solved by imposing proper boundary conditions for the scattering and absorbing medium.

It is clear that in order to solve Eq. (4.1), information about the optical depth which is related to the extinction cross section, the single-scattering albedo and the phase function desribed previously is needed. Once the diffuse intensity has been calculated from Eq. (4.1), the monochromatic upward and downward fluxes may then be evaluated by

$$F_\lambda^\uparrow(\tau) = \frac{1}{2} \int_0^1 I_\lambda(\tau, \mu) \mu d\mu \quad (4.2a)$$

$$F_\lambda^\downarrow(\tau) = \frac{1}{2} \int_0^{-1} I_\lambda(\tau, \mu) \mu d\mu + \mu_0 F_0 e^{-\tau/\mu_0}. \quad (4.2b)$$

Moreover, it is conventional in radiative transfer to define the radiative properties of a scattering and absorbing cloud layer in terms of nondimensional parameters. Let the optical depth of a cloud layer at the wavelength λ be τ_1 and assume that there is no atmosphere above and below such a layer. In the solar region, we define the reflection r and transmission t of the cloud layer in the forms

$$r_\lambda = F_\lambda^\uparrow(0)/\mu_0 F_{0\lambda} \quad (4.3a)$$

$$t_\lambda = F_\lambda^\downarrow(\tau_1)/\mu_0 F_{0\lambda}. \quad (4.3b)$$

Based on the conservation of radiative flux, i.e., without the external energy souce and since the internal emission in the solar spectrum can be ignored, the absorption α_λ is then given by $(1 - r_\lambda - t_\lambda)$.

2) THERMAL IR RADIATION

In the thermal infrared region, the equation of radiation transfer may be expressed by

$$\mu \frac{dI_\lambda(\tau, \mu)}{d\mu} = I_\lambda(\tau, \mu) - \frac{\tilde{\omega}_\lambda}{2} \int_{-1}^{1} P_\lambda(\mu, \mu') I_\lambda(\tau, \mu') d\mu' - (1 - \tilde{\omega}_\lambda) B_\lambda[T(\tau)] \quad (4.4)$$

where B_λ is the Planck radiance as a function of temperature T, and the last term represents the internal emission contribution to the diffuse intensity. This equation differs from Eq. (4.1) only in the source term. We define the cloud top and base emissivities corresponding to cloud top and base temperatures T_t and T_b, respectively, as follows:

$$\epsilon_\lambda^\uparrow = F_\lambda^\uparrow(0)/\pi B_\lambda(T_t) \quad (4.5a)$$

$$\epsilon_\lambda^\downarrow = F_\lambda^\downarrow(\tau_1)/\pi B_\lambda(T_b). \quad (4.5b)$$

If $T_t \approx T_b$, then one emissivity may be defined such that $\epsilon_\lambda \approx (\epsilon_\lambda^\uparrow + \epsilon_\lambda^\downarrow)/2$. Since the earth and the atmosphere below the cloud also emit energy and since the earth's surface temperature is generally higher than that of the cloud, it is necessary to consider the infrared reflectivity $\mathcal{R}_\lambda$ and transmissivity $\mathcal{T}_\lambda$ of the scattering and absorbing cloud layer due to radiative flux incident from below. Assuming that the upward flux reaching the cloud base is denoted by $F_\lambda^\uparrow(\tau_1)$ and that the emission from the cloud $B_\lambda(T)$ is set to be zero, then we write

$$\mathcal{R}_\lambda = F_\lambda^\downarrow(\tau_1)/F_\lambda^\uparrow(\tau_1) \quad (4.6a)$$

$$\mathcal{T}_\lambda = F_\lambda^\uparrow(0)/F_\lambda^\uparrow(\tau_1). \quad (4.6b)$$

Clearly, reflectivity is generated via the scattering of cloud particles. This is especially important for cirrus clouds which are composed of large ice crystals. Owing to the scattering processes, as well as the nonisothermal nature of the cloud, the concept of the local thermodynamic equilibrium, via the Kirchhoff law, is not applicable to the cirrus cloud layer as a unit.

One final note may be in order. It has been conventional knowledge that water clouds may be treated as blackbodies in the thermal infrared region. This is in view of the fact that high droplet number densities are generally observed in water clouds. Even a thin low stratus of a few hundred meters can be treated to a good approximation as a blackbody because of its high number density. The other physical aspect noted is that water droplets are normally quite small (<10 μm). Thus, their scattering effects with respect to the larger IR wavelengths are relatively small and probably could be ignored. Consequently, it appears physically appropriate to assume that localized portions of the water cloud are in thermodynamic equilibrium. However, high cirrus clouds, which are composed of large ice crystals with low number densities, are generally nonblack and cannot be described in the context of localized thermodynamic equilibrium so far as infrared emission is concerned.

Although methods developed for solving Eqs. (4.1) and (4.4) are numerous (e.g., see Lenoble, 1977; Liou,

1980), only limited studies have focused on the cirrus cloud problem. Assuming that cirrus clouds are composed of randomly oriented long cylinders and utilizing a modified two-stream approximation for radiative transfer, Liou (1973) reported reflection, transmission and absorption properties of cirrus cloud layers in the visible and near-infrared wavelengths. For the first time, the nonsphericity of ice crystals was incorporated into radiative transfer analysis. In the infrared region, Liou (1974) derived the transmissivity, reflectivity and emissivity of cirrus clouds in the 10 μm window by means of the discrete-ordinate method for radiative transfer. Stephens (1980a) also presented infrared emissivity and reflectivity in the window wavelength for cirrus clouds using the cylindrical scattering model and an adding method for radiative transfer. He indicated that the most significant difference between cylindrical and spherical models in the computation of infrared radiative properties involves the reflectivity which is important in the parameterization of the radiative properties of cirrus clouds. More recently, Wu (1984) discussed some aspects of parameterizing the cirrus IR emissivity in the 10 μm window wavelength. The effective emissivity is shown to be composed of effective absorption, scattering and reflective emissivities, which can be parameterized from basic cloud physics and radiative terms. On the experimental side, Platt and Gambling (1971) carried out combined ruby lidar and 10 μm window observations and found that the cirrus emissivity varies considerably over the period of measurement. In follow-up works, Platt (1973, 1975) reported more comprehensive observations of the cirrus emissivity in the 10 μm window and gave a value of $\sim$0.38. Recently, Platt et al. (1980) and Platt and Dilley (1981), based on satellite and lidar observations, estimated the cirrus emissivity and gave values from 0.2 to 0.95 with the corresponding albedo from 0.1 to 0.32. The foregoing values reported by Platt et al. represent a significant variability in the radiative properties of cirrus from an experimental perspective. For applications to remote sensing and atmospheric energetics, it is necessary that a physical correlation between the radiative and composition (and geometric) properties of cirrus clouds be established.

3) SOLAR RADIATION TRANSFER IN HORIZONTALLY ORIENTED ICE CRYSTALS

As discussed in the section on cloud composition, large ice crystals occurring in nature may have a preferred orientation. In addition, we pointed out in the light scattering section that the scattering phase function and extinction and scattering cross sections for horizontally oriented hexagons depend on the incident and emergent light beam. As a result of these complications, Eq. (4.1) is no longer valid in the solar radiation region. Liou (1980) undertook the theoretical formulation of the transfer of radiation in horizontally oriented ice crystals. If one defines the vertical ice path length in the form,

$$u = \int_0^z N(z')dz'$$

where N denotes the number density of the ice crystals, then the basic equation may be expressed by

$$\mu \frac{dI_\lambda(u;\mu,\phi)}{du} = -I_\lambda(u;\mu,\phi)\sigma_e(\mu) + \frac{1}{4\pi}\int_0^{2\pi}\int_{-1}^{1}\sigma_s(\mu')P_\lambda(\mu,\phi;\mu',\phi')I(u;\mu',\phi')d\mu'd\phi' + \frac{1}{4\pi}\sigma_s(-\mu_0)P_\lambda(\mu,\phi;-\mu_0,\phi_0)F_{0\lambda}e^{-\sigma_e(-\mu_0)(u_1-u)/\mu_0} \tag{4.7}$$

where ϕ denotes the azimuthal angle and the scattering and extinction cross sections, σ_s and σ_e are now functions of the incident angle. Also, the scattering phase function depends on the directions of the incoming and outgoing beams. If the single-scattering parameters are known through single-scattering calculations, a solution to the intensity distribution in a cloud composed of randomly oriented ice crystals in a horizontal plane may be obtained. Stephens (1980b) discussed some aspects of the transfer of solar radiation through ice clouds which are optically anisotropic. Asano (1983b) carried out a more detailed analysis of the transfer of solar radiation in ice clouds with the single-scattering properties varying with the incident angle of the light beam. It was shown that the reflection and transmission properties of cirrus clouds with optical depths ≤ 1 depend quite significantly on whether the ice crystals are oriented randomly in three-dimensional space or in a horizontal plane. Neither Stephens' nor Asano's analyses accounted for the scattering features produced by hexagonal crystals, however. Basically, what we need is the quantitative effects of horizontal orientation on the reflection and transmission properties of cirrus clouds in the solar region so that appropriate adjustments may be made for the flux and heating rate calculations involving cirrus.

c. *Broadband radiative flux transfer in cirrus cloudy atmospheres*

1) THEORETICAL ASPECTS

To apply the information on the light scattering and radiative transfer properties of cirrus clouds for practical atmospheric energetic studies, it is necessary to extend our discussion to cover the entire solar and thermal IR spectra and to understand the manner in which the cloud layers interact with absorbing gases in the atmosphere. In Fig. 12 we depict the solar and IR spectra and identify various absorbers in the graph.

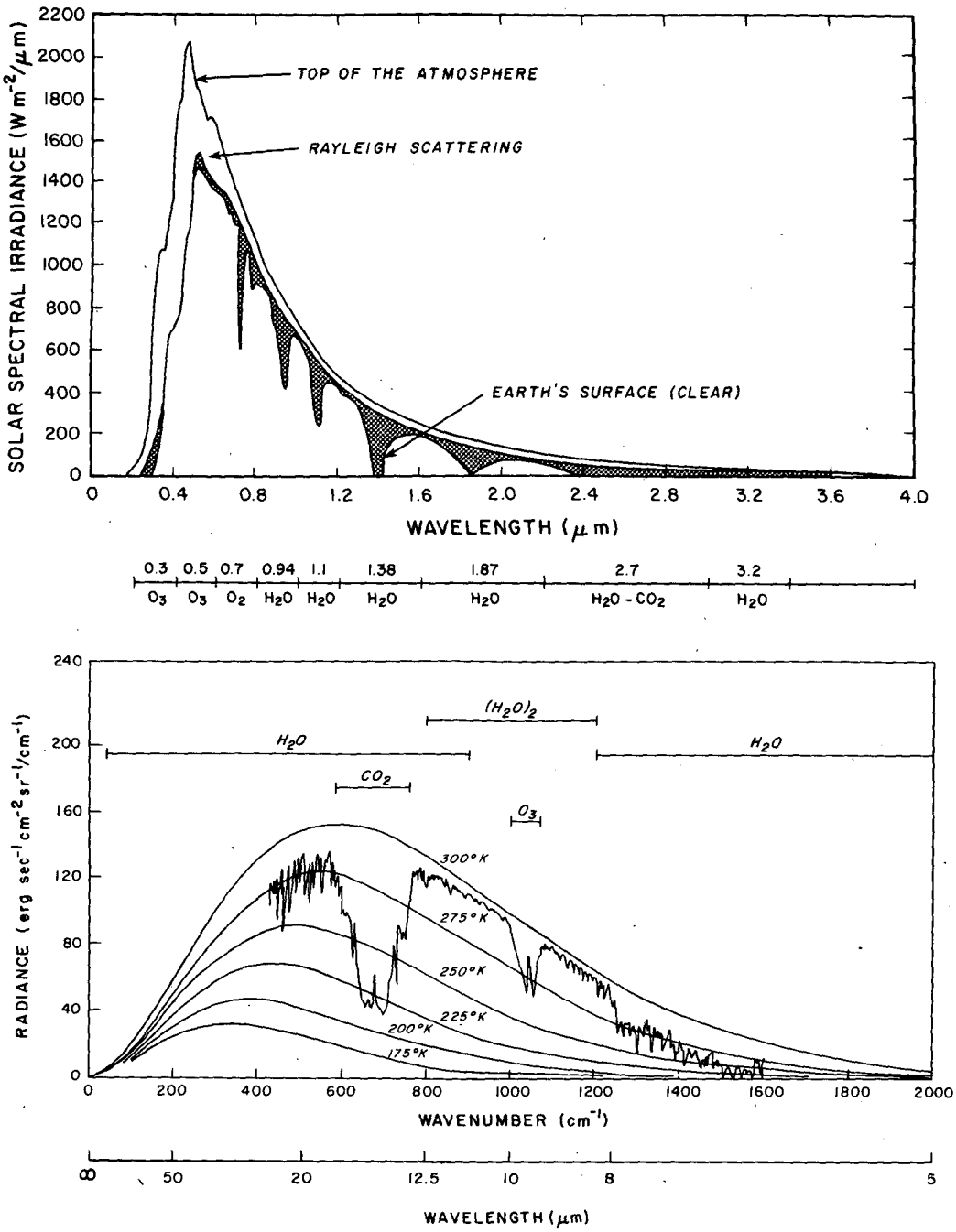

FIG. 12. Solar and thermal infrared absorption spectra. Major absorbers are depicted in these spectra.

While the real and imaginary parts of the refractive indices for ice vary slowly, the absorption lines corresponding to H_2O, CO_2 and O_3 are highly variable in the wavelength (or wavenumber) domain. In order to efficiently evaluate the transfer of solar and thermal IR fluxes in an atmosphere containing a cirrus cloud, the solar and IR spectra are divided into a number of intervals according to the position of the absorption bands of H_2O, CO_2 and O_3. The gaseous transmittances are then calculated for each band interval with appropriate pressure and temperature corrections to account for inhomogeneous atmospheric paths. Subsequently, exponential fittings are performed to get a set of equivalent absorption coefficients for the band so that the scattering and absorption contributions due to ice crystals may be properly included in the transfer calculations. This technique has been widely used for the incorporation of aerosol and cloud scattering contri-

butions in absorbing atmospheres (Liou and Sasamori, 1975; Ackerman et al., 1976; Feigelson, 1981; Wiscombe et al., 1984).

An alternative approach for the incorporation of scattering processes in absorbing atmospheres has been the use of the so-called k-distribution method originally developed by Arking and Grossman (1972) and further developed by Chou and Arking (1980, 1981). The method makes use of the fact that for a homogeneous atmosphere the transmittance within a relatively wide spectral interval is independent of the ordering of the value of the absorption coefficient k with respect to the wavenumber. However, it depends only on the fraction of the interval that is associated with a particular value of k. This fraction is simply a probability density function. In essence, this method is equivalent to the exponential fitting mentioned above from the numerical computation point of view.

Assuming that the methodology for the computation of the transfer of spectral bands in absorption and scattering atmospheres has been established, we may proceed to discuss the broadband radiative flux transfer. In reference to Eq. (4.2), the total upward and downward fluxes covering the entire solar or thermal IR spectrum may be written in the form

$$F^{\uparrow\downarrow}(p) = \int_0^\infty F_\lambda^{\uparrow\downarrow}(p)d\lambda \approx \sum_{i=1}^{N} F_{\lambda_i}^{\uparrow\downarrow}(p)\Delta\lambda_i \quad (4.8)$$

where N denotes the number of the spectral interval selected. Also, we have changed the τ-coordinate to the p (pressure) coordinate. In the solar region, the solar constant may be defined by $S = \int_0^\infty F_{0\lambda}d\lambda$. In the thermal region, the Stefan–Boltzmann's law gives $\sigma T^4 = \int_0^\infty \pi B_\lambda(T)d\lambda$. Consequently, broadband reflection and transmission in the solar region and broadband emissivity in the thermal IR region associated with cloud layers similar to those given in Eqs. (4.3), (4.5) and (4.6) may be properly defined.

Because of the complexity in the determination of the broadband thermal IR emissivity, a simplified approach has been used to approximate its value. Chylek and Ramaswamy (1982) and Stephens (1984) proposed the following exponential form for the monochromatic flux emissivity:

$$\epsilon_\lambda^f = \int_0^1 [1 - \exp(-k_\lambda^c W/\mu)]\mu d\mu \left[\int_0^1 \mu d\mu\right]^{-1} \approx 1 - \exp(-\beta k_\lambda^c W) \quad (4.9)$$

where k_λ^c is the mass extinction coefficient for cloud particles, W is the vertical liquid water content and $\beta \approx 1.66$ is known as the diffusivity factor. The expression defined in Eq. (4.9) accounts for absorption and single-scattering of cloud particles but it does not include the multiple scattering effects. For broadband applications, it has been argued that, since the variation of k_λ^c with wavelength is relatively smooth owing to the more continuous nature of water absorption compared to molecular absorption, the grey approximation may be applicable, viz.,

$$\epsilon^f \approx 1 - \exp(kW) \quad (4.10)$$

where $K = \beta k^c$ and k^c is the wavelength-averaged mass extinction coefficient which may be symbolically written

$$k^c = \int_0^\infty k_\lambda^c B_\lambda(T)d\lambda/\sigma T^4.$$

As stated above, the computation of the flux emissivity based on Eq. (4.10) is a physical simplification. Thus, for remote sensing and atmospheric energetic applications, the window and broadband flux emissivities computed from Eq. (4.10) are subject to verification. While a comprehensive comparison program for the cirrus emissivity derived from Eq. (4.10) and more exact radiative transfer programs has not been performed to the best of my knowledge, I suspect that Eq. (4.10) may be adequate for optically thin and moderately thick cirrus. For thick cirrus, multiple scattering effects intensify and the downward IR reflectivity becomes significant. Equation (4.10), which has a limiting value of 1 when $W \to \infty$, is not sufficient to account for the apparent (or effective) flux emissivity. Alternately, one may utilize measured data to get k^c, known as the effective absorption coefficient with conventional units of $cm^2\ g^{-1}$. Based on broadband flux measurements for cirrus clouds discussed below, Paltridge and Platt (1981) obtained a value of 0.056 for k^c, while Griffith et al. (1980) gave a range of 0.076 to 0.096 for k^c. As shown in Fig. 13, the variations of k^c between these two measurements are quite significant. In future experiments, a mean k^c should be narrowed down with a range of uncertainty given (see section 4c(2ii) and Fig. 14 for further discussion).

Conceivably, if solar and IR radiative properties for clouds can be calculated "exactly" under a number of atmospheric conditions, parameterizations may be carried out to define these properties in terms of some key cloud variables. One such cloud parameter for radiative transfer computational purposes has been identified as the vertical liquid water content. Liou (1976) obtained the reflection, transmission and absorption of solar radiation by cirrus cloud layers utilizing the discrete-ordinate method for radiative transfer. Further, Liou and Wittman (1979) presented a parameterization of the radiative properties of cirrus as functions of the solar zenith angle (in the solar region) and the ice-water content of cirrus in terms of known mathematical functions.

Kinne (private communication, 1985) carried out a more comprehensive parameterization on the radiative properties of cirrus clouds. In the calculation of the IR emissivity for climatic applications, he assumed that the averaged cirrus particle distribution is a combination of two size distributions for cirrus uncinus and

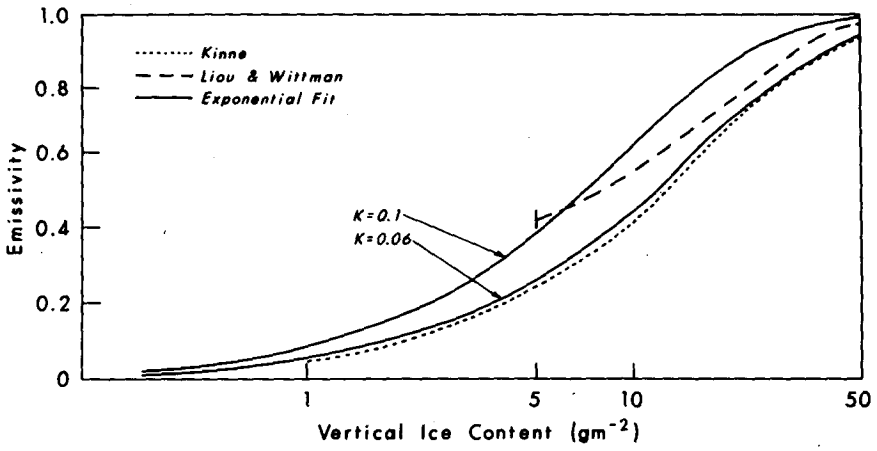

FIG. 13. The cirrus IR emissivity as a function of the vertical ice content from various theoretical sources.

cirrostratus derived by Heymsfield and depicted in Fig. 3. The IR emissivity curve as a function of the vertical ice content, based on detailed radiative transfer calculations, is shown in Fig. 13. In this figure, results from Liou and Wittman who used a polynomial fitting, and an exponential fit, i.e., $1 - \exp(-kW)$ with $k = 0.1$ and 0.06 discussed previously, are also depicted. Liou and Wittman's results are limited to a vertical content of ~ 5 g cm^{-2} and therefore are not applicable to very thin cirrus. Kinne's computational results based on radiative transfer, including multiple scattering, demonstrate that the IR emissivity follows closely with the exponential attenuation for the vertical ice content less than about 20 g m^{-2}. For the ice particle size distribution employed in the calculation, it appears that multiple scattering effects are important only for optically thick cirrus clouds. In order to apply these emissivity values for weather and climate studies, it is necessary to have a cirrus cloud model in which the ice content can be interactively computed.

2) AIRCRAFT OBSERVATIONS OF BROADBAND RADIATIVE FLUX IN CIRRUS CLOUDS

(i) *Solar radiation.* Aircraft measurements of broadband incoming (downward) and outgoing (upward) hemispherical solar fluxes at the cloud top and bottom allow the evaluation of the reflection, transmission and absorption of cloud layers. Let the total downward and upward fluxes at the cloud top (z_t) and base (z_b) be denoted by $F^{\downarrow}(z_t)$ and $F^{\uparrow}(z_t)$, and $F^{\downarrow}(z_b)$ and $F^{\uparrow}(z_b)$, respectively. Then the reflection and transmission of the solar radiation for a given solar zenith angle θ_0 are given by

$$r = F^{\uparrow}(z_t)/F^{\downarrow}(z_t) \tag{4.11}$$

$$t = F^{\downarrow}(z_b)/F^{\downarrow}(z_t). \tag{4.12}$$

And the cloud absorption may be obtained from the divergence of the net flux at the cloud top and base in the form

$$\alpha = \{[F^{\downarrow}(z_t) - F^{\uparrow}(z_t)] - [F^{\downarrow}(z_b) - F^{\uparrow}(z_b)]\}/F^{\downarrow}(z_t). \tag{4.13}$$

Employing the airborne Eppley precision spectral pyranometers, Drummond and Hickey (1971) derived a mean reflection of 20% for cirrus–cirrostratus clouds when the solar elevation angle was about 65°. Reynolds et al. (1975) analyzed the upward and downward solar flux data measured from aircraft during the Barbados Oceanographic and Meteorological Experiment (BOMEX). They illustrated that the reflection of thick cirrus clouds ranged from 47 to 59%, whereas absorption were, respectively, 13–14% and 27–40%. Their results clearly indicated the large variability in reflection and absorption of thick cirrus clouds, probably due to the change in the cloud composition and thickness. It is also interesting to note that the observed results of Reynolds et al. revealed that absorption of solar flux in the cloud-free troposphere was as large as 26%. Unfortunately, no detailed atmospheric water vapor profile and cloud composition and structure were recorded during the radiation experiment nor were the uncertainties of the aforementioned values derived from measurements assessed by these authors. More recently, Paltridge and Platt (1981) carried out aircraft measurements of solar and infrared radiation along with the microphysics for a number of cirrus cloud decks with thicknesses from 1.5 to 2.5 km. They reported solar absorption and reflection on the order of 0.14 and 0.4, respectively. Certainly, carefully designed field experiments involving radiation and cirrus cloud measurements should be carried out to narrow down the uncertainty in the solar radiative properties of cirrus clouds and to provide climatological mean and standard deviation of these properties according to latitudes.

(ii) *Thermal IR radiation.* The basic physical parameter associated with the cloud thermal IR radiation, which can be deduced from aircraft measurements of upward, $F^{\uparrow}_{IR}(z)$ and downward, $F^{\downarrow}_{IR}(z)$ broadband fluxes at a given height, is the so-called emissivity. Since the cloud temperature may vary significantly, two components involving upward and downward emissivities are defined by (Cox, 1976)

$$\epsilon^{\uparrow}(z_t) = [F^{\uparrow}(z_t) - F^{\uparrow}(z_b)]/[\sigma T_t^4 - F^{\uparrow}(z_b)] \quad (4.14a)$$

$$\epsilon^{\downarrow}(z_b) = [F^{\downarrow}(z_b) - F^{\downarrow}(z_t)]/[\sigma T_b^4 - F^{\downarrow}(z_t)]. \quad (4.14b)$$

The emissivities so defined are referred to as effective emissivities since they are defined in terms of measured flux densities which contain components due to scattering of cloud particles.

Griffith et al. (1980) carried out aircraft observations of the thermal IR radiative properties of tropical cirrus clouds and reported emissivities derived from the measurements. An interesting point derived from their data, and perhaps an important one from the radiative budget point of view, is that observed tropical cirrus clouds which have a geometric thickness within 1 km are generally optically thick with emissivities approaching unity. This study suggests that there may be significant spatial variations in the radiative properties of cirrus clouds.

The aforementioned paper by Paltridge and Platt (1981) also measured the broadband IR emissivity of cirrus clouds with detailed supporting data on ice crystal characteristics. Figure 14 depicts the broadband emissivity as a function of the vertical ice–water content. The solid curve is the best exponential fit to the data using Eq. (4.10) with $K = 0.056$. In comparison to Fig. 13, it is noted that the theoretical results depicted in that figure are all within the uncertainty of observed data. The data presented by Paltridge and Platt, as well as by Platt and his coworkers cited in 4b(2) illustrates that individual cirrus emissivity varies significantly with a value ranging from about 0.1 to 0.9. As will be discussed below, thermal equilibrium temperature profiles are extremely sensitive to the cirrus emissivity values assumed in climate models. Thus, for applications to climate problems and climate modeling, it is important to derive a reliable global cirrus IR emissivity in terms of its mean and variance.

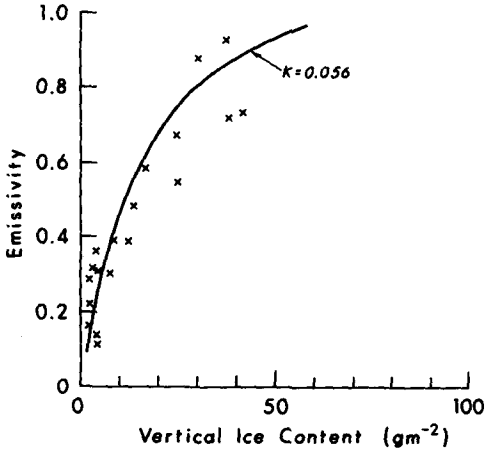

FIG. 14. As in Fig. 13 but from aircraft observations. (After Paltridge and Platt, 1981 with modifications.)

d. *Solar and IR heating rates in cirrus cloudy atmospheres*

Radiative processes influence the dynamics and thermodynamics of the atmosphere directly through the generation of radiative heating and cooling rates as well as net radiative fluxes available at the surface. Obviously, the radiative flux exchange is largely controlled by the cloud field in general and cirrus clouds in particular. We begin our discussion on the definition of the radiative heating/cooling rates with the basic thermodynamic equation which may be written in the pressure coordinate in the form

$$\frac{\partial T}{\partial t} + \frac{u}{a\sin\theta}\frac{\partial T}{\partial \lambda} + \frac{v}{a}\frac{\partial T}{\partial \theta} + \omega\left(\frac{\partial T}{\partial p} - \frac{RT}{C_p P}\right) = Q^C + Q^R + F^T + g\frac{\partial \tau^T}{\partial p} \quad (4.15)$$

where λ is the longitude, θ the co-latitude, a the radius of the earth, Q^C the latent heat, Q^R the radiative heating, F^T the horizontal eddy nonlinear viscosity for temperature, τ^T the vertical eddy sensible heat flux, and other notations are conventional. The radiative heating is generated through solar and thermal IR flux exchanges in the atmosphere and may be expressed by

$$Q^R = Q_S - Q_{IR} = \frac{g}{C_p}\frac{\partial}{\partial p}(F_S - F_{IR}). \quad (4.16)$$

Under partly cloudy conditions, the solar heating and IR cooling rates Q_S and Q_{IR} are given by

$$Q_{S,IR} = \eta Q^{c}_{S,IR} + (1 - \eta)Q^{nc}_{S,IR} \quad (4.17)$$

where η denotes the cloud cover and the superscripts c and nc represent cloud and no-cloud conditions, respectively.

Fleming and Cox (1974) investigated the infrared radiative properties of cirrus clouds and illustrated the importance of cirrus on the heat budget in the tropics. The influence of cirrus clouds on the infrared cooling rate of the troposphere and lower stratosphere was investigated by Roewe and Liou (1978). They showed that cirrus clouds strongly suppress tropospheric cooling and significantly increase cooling in the stratosphere above 20 km and that the presence of low-level clouds significantly modifies the cooling within the cirrus cloud. Freeman and Liou (1979) constructed a comprehensive radiative balance model to examine the ef-

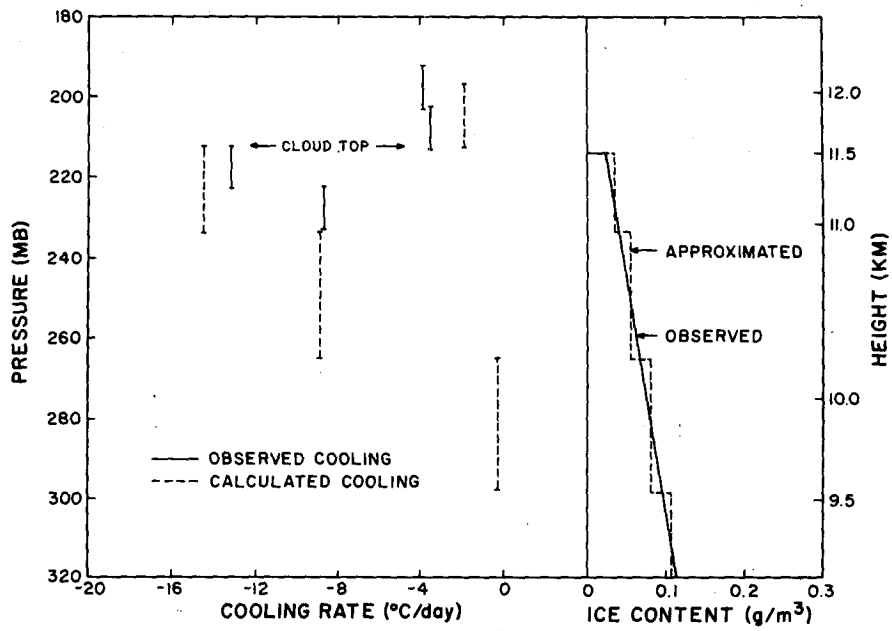

FIG. 15. Comparison of observed and calculated cooling rates within a thick cirrus. The observed values were taken from the report by Griffith and Cox (1977). Also illustrated are the observed and approximated vertical profiles of ice content.

fects of the increase of cirrus cloud cover on atmospheric heating and cooling profiles and assessed the climatic impact from the radiative transfer point of view.

Roewe and Liou (1978) computed the IR cooling rates within a thick cirrus and compared them with measured values from the GATE project presented by Griffith and Cox (1977). The observed flux and cloud particle data were collected by the NCAR Sabreliner during August and September 1974 in the tropical region. On the right of Fig. 15 is shown the derived vertical profile of the ice content within the cirrus for 8 September 1974 reported by Griffith and Cox. The left side of this figure illustrates the measured cooling rates for this particular day. The calculated cooling rate corresponds to an averaged value for a 1 km thick cloud. The averaged cooling rate at the cloud top layer is seen to be $\sim 8°C\ day^{-1}$ from both theoretical calculations and field observations. Near the cloud base (the cloud base height was not reported), the averaged cooling rate is greatly suppressed. The rather random fluctuations in the measured cooling reveal that the vertical profile of the ice content may be more complex than the given curve indicates. These results show that there is a general agreement between calculated and observed cooling rates.

In Fig. 16, we present infrared cooling (lower diagrams) and solar heating (upper diagrams) rates for a number of cirrus cloudy atmospheres using standard atmospheric temperature, water vapor and ozone profiles computed from a comprehensive radiative transfer program developed at the University of Utah in which heating and cooling rates within the cirrus are also evaluated. Cirrus clouds with thicknesses of 0.1, 1 and 3 km are inserted in the atmosphere and a 100% cloud cover is assumed. The base of these clouds is fixed at 8 km. The mean ice content employed in the calculation is 0.013 g m^{-3} which gives these clouds vertical ice contents of, respectively, 1.3, 13 and 39 g m^{-2}. The extinction coefficients at the 0.55 μm visible and 10 μm IR wavelengths for ice crystals are, respectively, 0.667 and 0.740 km^{-1}. For calculations of solar flux transfer, we employ a solar constant of 1360 W m^{-2}, a surface albedo of 0.15, a cosine of the solar zenith angle of 0.5 and a solar time duration of 12 h. These values represent mean solar conditions so that the resulting solar heating may be directly compared with the thermal IR cooling. In a clear atmosphere, maximum cooling rates on the order of $2°C\ day^{-1}$ are seen near the ground. Another maximum is located at about 5 km due to the structure of temperature and water vapor profiles. Cooling rates decrease to a height of about 12 km and then increase as a function of height due to carbon dioxide and ozone emission. In general, we see cooling outweighs heating everywhere in a clear troposphere by about $1–2°C\ day^{-1}$.

When a cirrus with a thickness of 0.1 km and a base height of 8 km is inserted in the atmosphere, the solar heating rate generated at the position of the cloud is $\sim 2°C\ day^{-1}$ but the heating below the cirrus remains largely unchanged. The cooling rate, on the other hand, is $\sim 3°C\ day^{-1}$ with small, but noticeable suppression

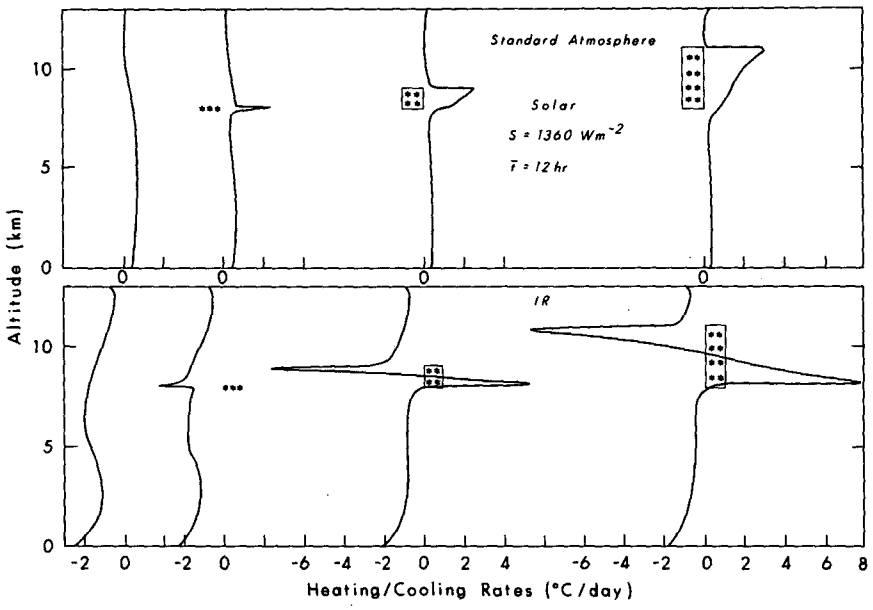

FIG. 16. Thermal IR and solar heating rates for cirrus cloudy atmospheres with cirrus thicknesses of 0, 0.1, 1 and 3 km. The cirrus base height is placed at 8 km, and the atmospheric profiles employed correspond to standard conditions.

of cooling below the cloud. In the 1 km cirrus case, the solar heating rate (note that this heating rate is a daily averaged value and does not represent the instantaneous solar heating at a given time interval during the day) has a maximum of $\sim 2.5°C\ day^{-1}$ at the cloud top. The IR counterpart shows a large cooling rate of $\sim 7.5°C\ day^{-1}$ at the cloud top generated by the cloud emission. At the cloud base, on the contrary, a significant heating of $\sim 5°C\ day^{-1}$ is observed which is produced from the trapping of atmospheric upward fluxes by the cloud. Significant suppression of the cooling below the cloud is also evident. For the thick cirrus having a vertical extent of 3 km, the solar heating at the cloud top is $\sim 3°C$ day. But cooling and heating profiles within the cloud vary from $-8.5°$ to $+7.5°C\ day^{-1}$. On the average, it is anticipated that the top of a thick cirrus will undergo strong cooling whereas at its base large heating will take place. In comparison with results presented in Fig. 15, it should be noted that the mean ice content used in the present calculation is 0.013 g m^{-3}. As a result of the smaller ice content employed, the cooling and heating rates at the cloud top and base, respectively, are smaller than those produced by a thick tropical cirrus.

Except for those presented by Griffith and Cox (1977) and analyzed more comprehensively by Griffith et al. (1980), there have been practically no cooling rate measurements carried out involving cirrus clouds. Moreover, to the best of my knowledge, solar heating rates in cirrus cloudy conditions have not been carefully analyzed from aircraft measurements. As is clearly depicted in Fig. 16, based on theoretical computations, cirrus clouds will generate a significant vertical inhomogeneity with respect to heating rates. Also clearly demonstrated in this figure is the significant horizontal heating differential produced by the presence of cirrus clouds. In what manner these vertical and horizontal heating differentials will influence the dynamic processes and the consequence of the temperature distribution is still a mystery. Also, how cirrus clouds play a role in the energy exchange between the troposphere and stratosphere is largely unknown. Of course, whether the heating and cooling profiles presented here are representative of those in realistic atmospheres should be checked and verified from comprehensive field programs involving detailed cloud and radiation measurements.

With respect to the application of heating and cooling rate calculations to numerical models for weather and climate studies, it should be pointed out that model calculations are subject to the vertical and horizontal discretization utilized. Since cirrus are generally subgrid clouds in the vertical (as well as horizontal), computing heating and cooling rates efficiently once the cloud is defined appears to be an area requiring a series of numerical experiments so that their effects can be properly incorporated into a model setting.

5. Numerical experiments on the effects of cirrus clouds on weather and climate

It has been recognized that clouds, which constantly cover $\sim 50\%$ over the global sky, are the most important regulators of the radiation balance of the earth–

atmosphere system. While clouds reflect a significant portion of incoming solar fluxes, they also trap the outgoing thermal infrared fluxes emitted from the earth's surface and lower troposphere. The prevalence of the solar albedo effect versus the IR greenhouse effect determines the gain or loss of radiative energy during a specific climate change which leads to warming or cooling of the earth–atmosphere system. These two effects on the local scale obviously depend on the specific earth–atmosphere conditions under which the clouds are embedded and their geometrical configuration and physical composition. In addition, various feedback mechanisms such as the humidity, coverage of ice/snow, and dynamic transport when coupled with clouds also affect the thermodynamic equilibrium of the atmosphere in an intricate way. Indeed, clouds remain one of the least understood atmospheric components of weather and climate systems.

In recent years, a number of studies have focused on the subject of the cloud–radiation interaction utilizing radiation budget data derived from satellites. Hartmann and Short (1980), Herman et al. (1980) and Ohring and Clapp (1980) attempted to determine the relative importance of the solar albedo and IR greenhouse effects due to the presence of clouds. While these analyses illustrate that the solar albedo effect is greater than the IR greenhouse effect at the top of the atmosphere with respect to variations in the fractional cloud coverage, the degree and extent to which these two affect the thermal structure of the earth–atmosphere system have not been quantified. Moreover, in what manner clouds might be influenced by external and internal radiative perturbations such as the anticipated increase of CO_2 concentration and solar constant variations, and how in turn they would affect the response to these perturbations are still physically unknown at this point.

As pointed out previously, clouds composed of water droplets are generally optically thick and, therefore, it is physically appropriate to assume these clouds to be blackbodies in the thermal infrared region. It would appear therefore, that the solar albedo effect in the case of water clouds will produce greater variabilities in the radiative budget of the atmosphere due to changes in the cloud vertical liquid water content. Charlock (1982) demonstrated the importance of the solar radiative properties of water clouds to the sensitivity of climatic temperature perturbations. The solar albedo effects due to water clouds are especially evident for the marine stratus and stratocumulus since their emitting temperatures are very close to those of the underlying ocean surface.

On the other hand, high level cirrus clouds, which contain a significant amount of large, nonspherical ice crystals in low concentrations, are normally optically thin and nonblack, as previously discussed. Because of their high location in the atmosphere and low reflection of the incoming solar fluxes, it has been physically recognized that the presence of cirrus clouds will normally produce a greenhouse effect from their downward emission. In the preceding sections, we have attempted to collect and discuss relevant microphysics, dynamics, and radiative properties of cirrus clouds in a logical and coherent manner. To place these into proper perspective with respect to their influence on global weather and climate systems, we shall describe sensitivity experiments utilizing numerical models which have been performed for investigating the effects of cirrus clouds on the thermal and dynamic structure of the earth–atmosphere system. We shall begin with the simplest one-dimensional radiative–convective model.

a. One-dimensional climate model

In their pioneering paper, which introduced the so-called convective adjustment for climate models, Manabe and Strickler (1964) discussed in some detail the role of high cirrus clouds in the thermal equilibrium temperature calculation. Using a simplified parameterization scheme for the transfer of solar radiation through cloud layers, Manabe and Strickler showed that if cirrus clouds have a solar reflection of 0.2 and an IR emissivity of 0.5 and if they are located above about 9 km, those cirrus clouds would exert a heating effect on the earth's surface. The height of cirrus clouds was found to be the fundamental reason for the heating. Manabe (1975) discussed the effect of contrails on the earth's surface temperature and pointed out the importance of cirrus blackness to the sensitivity of the surface equilibrium temperature. Manabe also pointed out the necessity of deriving reliable radiative properties of ice clouds in conjunction with climate studies. Based on the observed infrared emissivity, Cox (1971) argued that cirrus clouds may act to cool or warm the troposphere, depending on their emissivity values. Although Cox's conclusion was not derived from a numerical modeling study, it serves to indicate the importance of the cirrus emissivity in relation to climate studies.

It is quite clear from the preceding discussion that there are two basic cirrus parameters which may exert a significant influence on the earth's climate and climate changes, namely, the cirrus emissivity and height in the atmosphere. From a global perspective, it is noted that the latitudinal dependence of the cirrus cloud cover and the underlying surface albedo will also play an important role in the climate problem involving cirrus clouds. In a recent paper by Liou and Gebhart (1982), extensive one-dimensional numerical experiments were carried out to study the effect of cirrus clouds on the equilibrium temperature using a mean annual condition for the solar constant, solar zenith angle, sunlight duration, surface albedo, and with a number of humidity profiles. Cirrus thicknesses of 0.1, 1 and 3 km corresponding to vertical ice contents of 5.18, 51.8 and 156.8 g m^{-2} were used in the calculation. These values correspond to an assumed ice content of $\sim$0.05 g m^{-3}

which is about a factor of 4 larger than that employed in the calculations of the heating/cooling rates presented in Fig. 16. The larger ice content value used is probably valid for tropical conditions. In that paper, the computed solar albedo is only ~9% for the 0.1 km case, but such a cloud is already half-black in the thermal IR region. It was also noted that a cloud with a thickness of ≥3 km is practically a black cloud.

Figure 17a shows the thermal equilibrium temperatures for clear and various cirrus cloudy atmospheres using a tropical humidity profile. The cloud base in this graph is placed at 8 km. Temperatures increase significantly below the tropopause (at ~20 km) when a 0.1 km thin cirrus is inserted in the atmosphere. This is caused by a combination of the large solar flux transmission and thermal infrared greenhouse effect. The result of the thin high cloud effect on equilibrium temperatures derived in this study is in qualitative agreement with that presented earlier by Manabe and Strickler (1964) and more recently by Stephens and Webster (1981). As the cloud thickness increases, the atmospheric temperature reduces due to a significant decrease in solar fluxes. For clouds approaching blackbodies, we see lower temperatures above about 15 km. This is because lower cloud top temperatures act as surface emitters. Although the difference between the infrared radiative properties for the 1 and 3 km cloud cases are rather small, the temperature differences in the two cases are on the order of 10°K below about 15 km due to the difference in the solar radiation properties. The effects of the cloud location in the atmosphere on the thermal equilibrium temperature are shown in Fig. 17b where the cloud base is lowered to 5 km. When the half-black thin cloud is lowered from 8 to 5 km, equilibrium temperatures vary only slightly. However, when the thick cloud is moved to the lower atmosphere, equilibrium temperatures decrease drastically. For the cloud base in the 5 km case, the presence of a 1 km thick cloud shows small warming with respect to the clear atmosphere. The presence of a 3 km thick cloud, on the other hand, produces cooling everywhere in the atmosphere. Clearly, a thick cirrus behaves just like a water cloud in the thermal infrared region, although a portion of the solar fluxes may transmit through it.

b. Two-dimensional climate model

Two-dimensional climate models are basically designed to close the gap between three-dimensional general circulation models for climate studies and one-dimensional radiative–convective and energy balance climate models. Utilizing a two-dimensional model, Potter et al. (1978) presented some simulation results for the model performance. However, the details of radiation and dynamic parameterizations in the model were not presented in the literature. Peng et al. (1982) described a two-dimensional climate model which was intended for the thermal response to climate changes due to doubling of CO_2 and solar constant variations

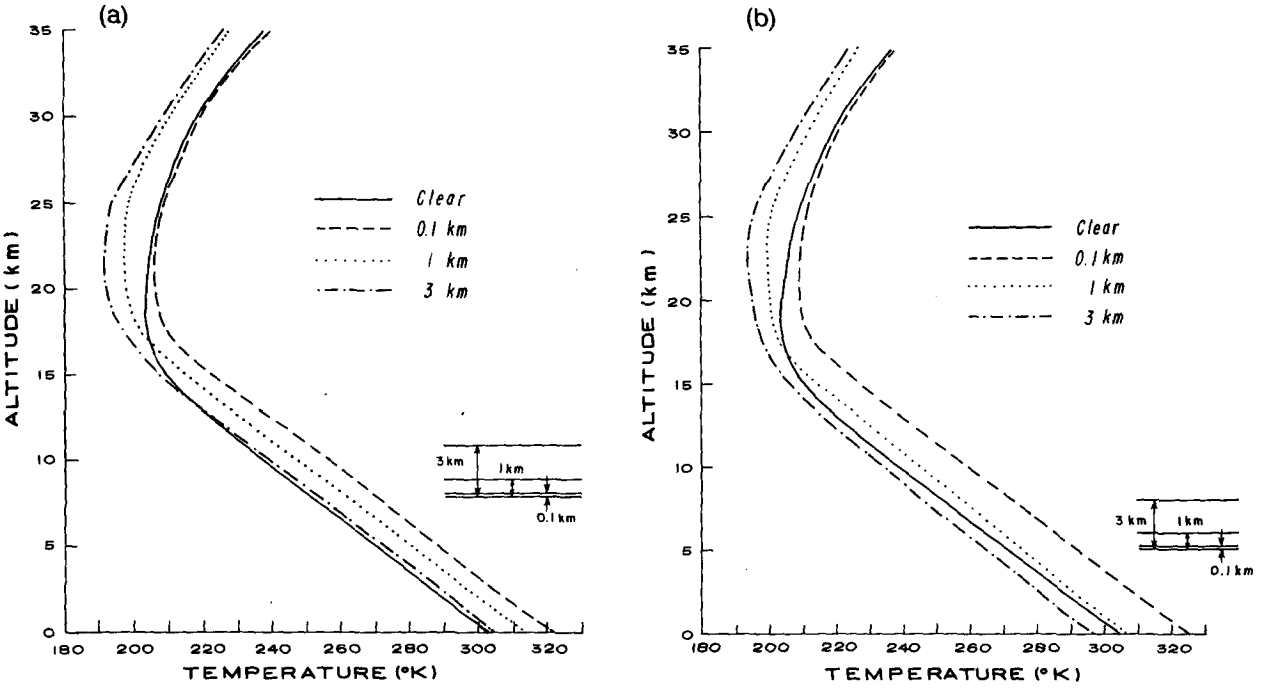

Fig. 17. Effects of the cirrus, (a) cloud thickness (or ice content) and (b) height on the thermal equilibrium temperature in a one-dimensional climate model. (After Liou and Gebhart, 1982.)

(Chou et al., 1982). More recently, Ou and Liou (1984) constructed a two-dimensional climate model based on the concept of the thermodynamic energy balance which is designed specifically for the investigations of the interactions of cloud–radiation and dynamic processes. The model consists of feedbacks caused by surface albedo and humidity variations, as well as feedbacks due to horizontal dynamic transports as functions of latitude.

In the previous subsection, the importance of the cirrus cloud emissivity and height to the thermal perturbation in dynamic and climate systems is pointed out. To gain a quantitative measure of the sensitivity of these two parameters to the zonally averaged temperature field, two numerical experiments have been undertaken employing Ou and Liou's model. One is concerned with the deviations of the climatological mean cirrus emissivity, while the other is associated with the changes of the climatological cirrus heights depicted in Fig. 9. With respect to the first experiments, the cirrus IR emissivity as a function of the vertical ice content and in relation to the solar reflection and transmission is depicted in Fig. 18. The vertical dashed line at the flux emissivity of 0.47 is assumed to be the climatological mean cirrus emissivity. The solar reflectance (or albedo) and transmittance, respectively, decreases and increases gradually, with respect to the increase of the IR emissivity ϵ. When it approaches unity, the solar albedo r_s increases drastically. Thus, for a thin cloud, it is expected that $\partial r_s/\partial \epsilon \ll 1$, whereas for a thick cloud close to black, we must have $\partial r_s/\partial \epsilon \gg 1$. The quantity $\partial r_s/\partial \epsilon$ is related to the competition between the solar albedo and the greenhouse effect. The cirrus radiative properties depicted in this figure are also related to the vertical ice content in units of g m^{-2}. At a visible wavelength of 0.55 μm, the optical depth for a cirrus with a thickness of 1.7 km having a vertical ice content of 5.7 g m^{-2} is about 0.5.

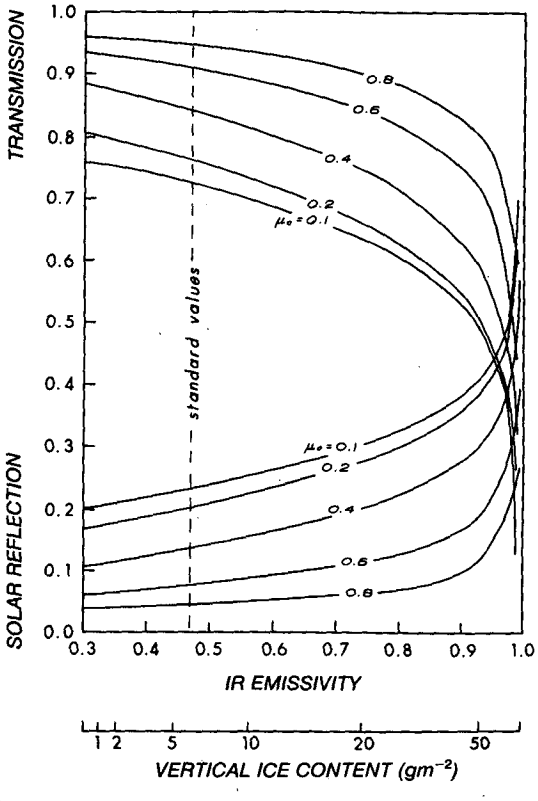

FIG. 18. The relationship between the solar reflection (albedo)/transmission and IR emissivity for cirrus clouds; μ_0 denotes the cosine of the solar zenith angle. The vertical dashed line at $\epsilon_0 = 0.47$ represents the cirrus IR emissivity determined from climatology data. (After Ou and Liou, 1984.)

Perturbations of the cirrus IR emissivity were carried out by uniformly increasing and decreasing its assumed climatological value from 0.47 to 0.57 and 0.32, respectively. As shown in Fig. 14, these emissivities are within reasonable range of the observed values. On the right of Fig. 19, increasing the cirrus IR emissivity from 0.47 to 0.57 produces significant warming of the troposphere. In the arctic region, the large increase in the temperature is due to the ice-albedo feedback. The humidity feedback mechanism also amplifies the temperature increases in the tropical troposphere. In addition, the meridional transports of sensible and latent heat fluxes by means of eddy and mean motions causes the temperature increase in the troposphere to be more homogeneous. The basic reason for the temperature increase is that additional downward fluxes are emitted from a blacker cirrus, while solar fluxes available below the cloud remain essentially unchanged. Subsequently, amplifications of the temperature increases by humidity, ice-albedo, and dynamic transport feedbacks take place which lead to the equilibrium temperature deviations depicted in the graph. On the left of Fig. 19, lowering the cirrus emissivity from 0.47 to 0.32, a 15% decrease, reverses the mechanisms described previously and leads to significant cooling patterns which resemble the heating patterns on the right, although the temperature decreases are larger due to a greater decrease in the emissivity. It is interesting to note that reasonable perturbations in the cirrus IR emissivity will produce temperature changes on the order of those due to doubling of CO_2 and a 2% increase in the solar constant (Manabe and Wetherald, 1980; Wetherald and Manabe, 1975).

Next, we investigate the sensitivity of cirrus cloud height variations to the equilibrium temperature. To avoid partial cloudiness in the vertical, the numerical experiments were done by raising and lowering the climatological cirrus cloud height, which is located at about 300 mb (Fig. 9), by one model layer. In effect, the cirrus base heights were moved to approximately 200 and 400 mb, respectively. In these experiments the cirrus IR emissivity is fixed at 0.47. In reference to the diagram on the right of Fig. 20, raising the cirrus clouds in the atmosphere produces warming in the troposphere as well as the stratosphere. The temperature in-

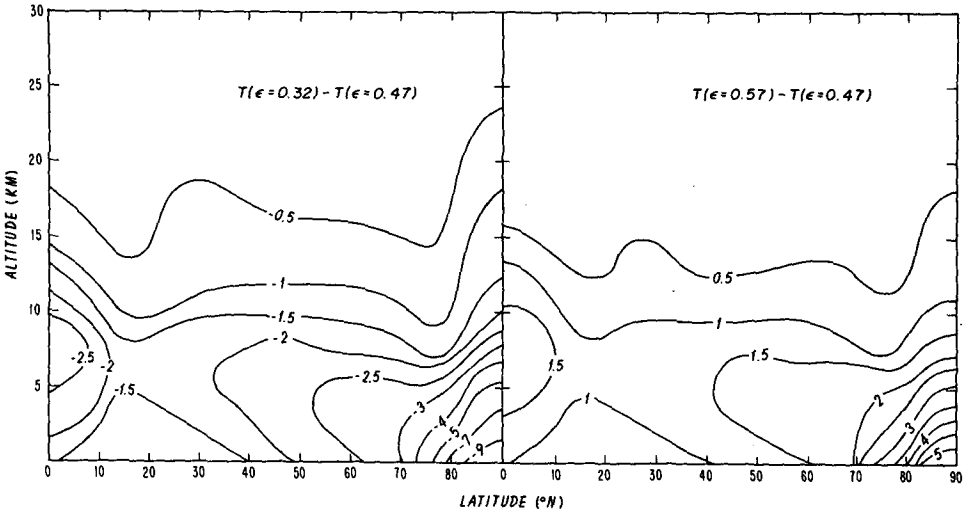

FIG. 19. The latitude–height distribution of temperature changes caused by a decrease (left) and increase (right) of the cirrus IR emissivity.

crease below the cloud is largely caused by the additional water vapor path length which increases the downward IR flux, plus the additional absorption of solar fluxes immediately beneath the cloud. We note that raising the cloud by 100 mb will result in a slight reduction of its downward emission because of lower cloud temperatures. However, the water vapor absorption and emission effects are predominant, resulting in a positive sensitivity to the temperature perturbations. Above the cloud, we also observe temperature increases which are generated by the increase of net fluxes. This increase is a result of the reduction of the upward IR emission from the colder cloud. The temperature increase is particularly evident in the tropics (<15°N) due to the combined amplification effects of cirrus and moisture. In comparison with Fig. 24 (right), the albedo feedback is less pronounced since the water vapor concentration in the arctic region is relatively small to allow a significant amplification to take place. Feedback consideration due to the transport of sensible and latent heat by mean and eddy motions reduces the gradient of temperature increases between the tropics and the arctic region. It is noted that cloud feedbacks in the meridional direction cannot be simulated in a one-dimensional setting. Finally, on the left of Fig. 20, we see that when cirrus is lowered by 100 mb, reverse temperature perturbations, i.e., temperature decreases are shown. Because of nonlinear interactions and feed-

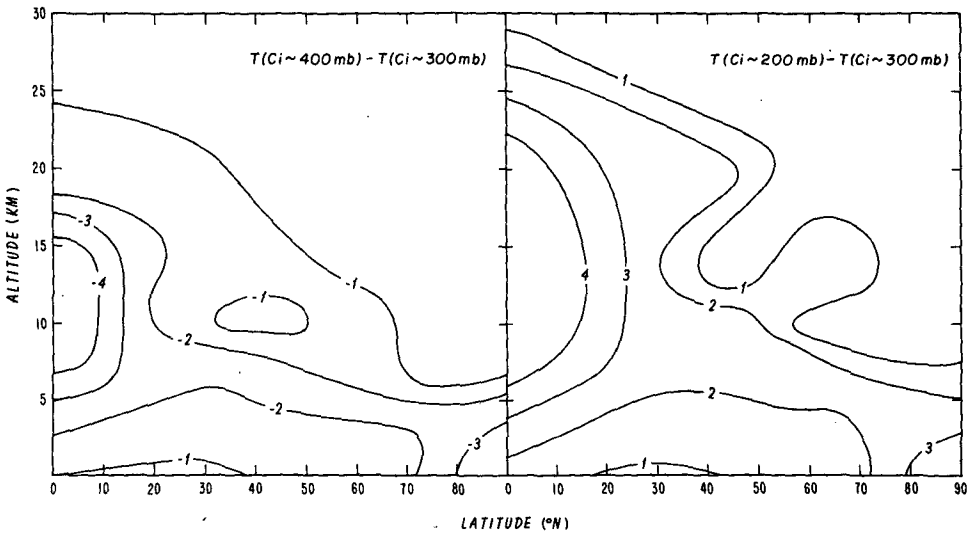

FIG. 20. As in Fig. 19 but caused by lowering (left) and raising (right) the cirrus height.

backs, the latitudinal pattern differs somewhat from the right figure.

In light of these sensitivity exercises, it is quite clear that accurate climatological cirrus IR emissivities and cirrus heights, perhaps as functions of latitude, are needed to construct a reliable climate model. Such a model may then be effectively utilized for the performance of numerical experiments for the physical understanding of the cause and effect relationship of external and internal radiative perturbations, including variations of the solar constant, increase of CO_2 concentration, volcanic dust and changes in the land surface characteristics. Finally, a predictive cirrus cloud model is needed to physically investigate the cirrus feedback processes, as previously noted in section 3c.

c. General circulation model

Numerous speculations have been made about the influence of the cloud variation on the sensitivity of climate by using general circulation models. Smagorinsky (1978) suggested that the increase in downward IR fluxes due to the CO_2 increase will enhance evaporation from the earth's surface which in turn will increase the amount of low clouds and thus will exert a cooling effect on the climate. Thus, the possible warming effects of the CO_2 increase may be compensated for by this negative feedback process. Roads (1978) and Schneider et al. (1978), on the other hand, speculated that the cloud variations may have a positive feedback effect on the sensitivity of the global mean climate. Roads specifically indicated from his experiments that higher sea surface temperature resulting in larger variance of the vertical velocity and greater efficiency of moisture removal through precipitation lead to a lower relative humidity and less cloudiness.

More recently, Wetherald and Manabe (1980) conducted a numerical experiment specifically designed for the study of the cloud cover sensitivity on climate. An idealized general circulation model was utilized, in which the distribution of cloud cover is a prognostic variable. They concluded that the influence of the cloud-feedback mechanism on the sensitivity of the global-mean climate may not be as large as originally suspected because of the compensation of the solar albedo and IR greenhouse effects, which we have discussed in previous subsections. However, they also pointed out that their method of cloud prediction is highly idealized and the radiative properties of various cloud types generated in their model may not be sufficiently realistic and adequate for the investigation of cloud–radiation interaction and feedbacks. In particular, the radiative problems of cirrus clouds have not been detailed in relation to climate and climatic perturbations.

In a recent paper, Ramanathan et al. (1983) demonstrated the possibility of improving the mean zonal simulation by virtue of refinements and improvements in radiative processes within the context of a general circulation model. Specifically, they showed that the radiative properties of cirrus clouds may have a direct impact on the general circulation of the model atmosphere. In their NCAR community climate model, the zonal averages of the computed zonal winds and temperatures for the standard condition, i.e., the control run, compared quite well with several of the observed features of the January zonal mean circulation. In the control run, the clouds were not permitted to form at altitudes above 250 mb between the equator and 45° and above 400 mb poleward of 45° so that radiatively active high level cirrus clouds were eliminated arbitrarily in the model control experiment. Ramanathan et al. then investigated the sensitivity of this model to the nonblack emissivity of cirrus clouds, assuming that their IR emissivity is given by Eq. (4.10), discussed in section 4, with the wavelength integrated absorption coefficient assumed to be 0.1 $(g\ m^{-2})^{-1}$. This is referred to as the variable nonblack cirrus (VNBC) experiment, while the other experiment, referred to as the variable black cirrus (VBC), assumed the clouds to be black in all layers. Figure 21 shows the zonal mean winds produced for these two experiments. In the VBC, both the winter and summer jets increase in strength unrealistically when compared with the results from the control run. But in the VNBC, the simulated summer hemisphere jet is in much closer agreement with the observed value. Although their control run was not performed with more realistic cloud formations in upper levels and IR emissivity coupling, the aforementioned two experiments suffice to reveal the importance of the radiative properties of cirrus clouds in general circulation models designed for climate sensitivity experiments.

As noted before, the relative importance to climate problems of the interactions and feedbacks of radiative transfer in clouds in general, and cirrus clouds in particular, has been physically recognized. However, the relevance of these processes to medium range weather prediction and the extent and degree to which prediction improvements can be made by the consistent integration of cloud–radiation processes in general circulation models are questions still open for scientific investigation and debate. In an attempt to understand the intricate interactions of radiation, clouds, and dynamic processes, Liou and Zheng (1984) carried out numerical experiments using a general circulation model that is appropriate for the performance of short and medium range weather prediction. Amid numerous findings concerning the quantitative effects of radiative transfer and cloud–radiation interactions on temperature and cloud prediction in a 10-day prediction experiment for the Northern Hemisphere, they illustrated that features of the general circulation of the model atmosphere are related to whether or not radiative transfer programs are included in the model. In the lower and upper diagrams of Fig. 22 are shown the

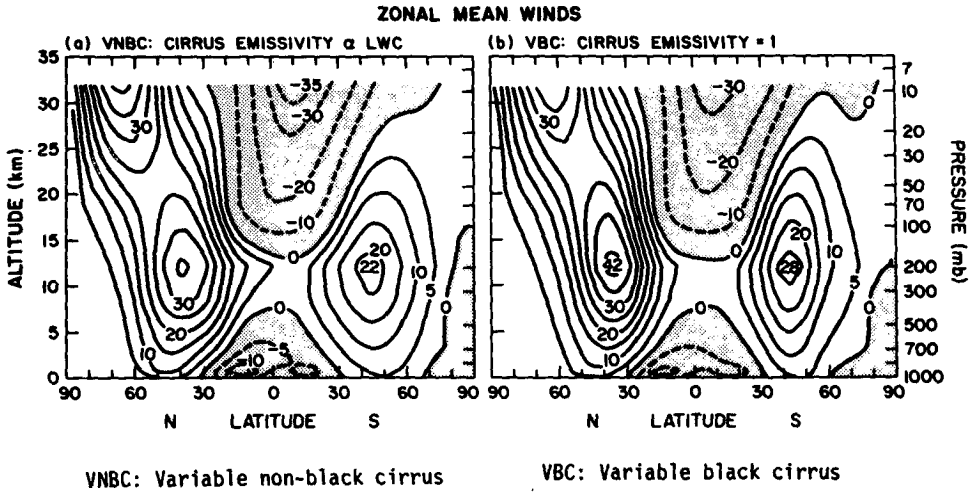

FIG. 21. Zonal mean winds generated from a GCM for (a) variable nonblack cirrus (VNBC) and (b) variable black cirrus (VBC). (After Ramanathan et al., 1983.)

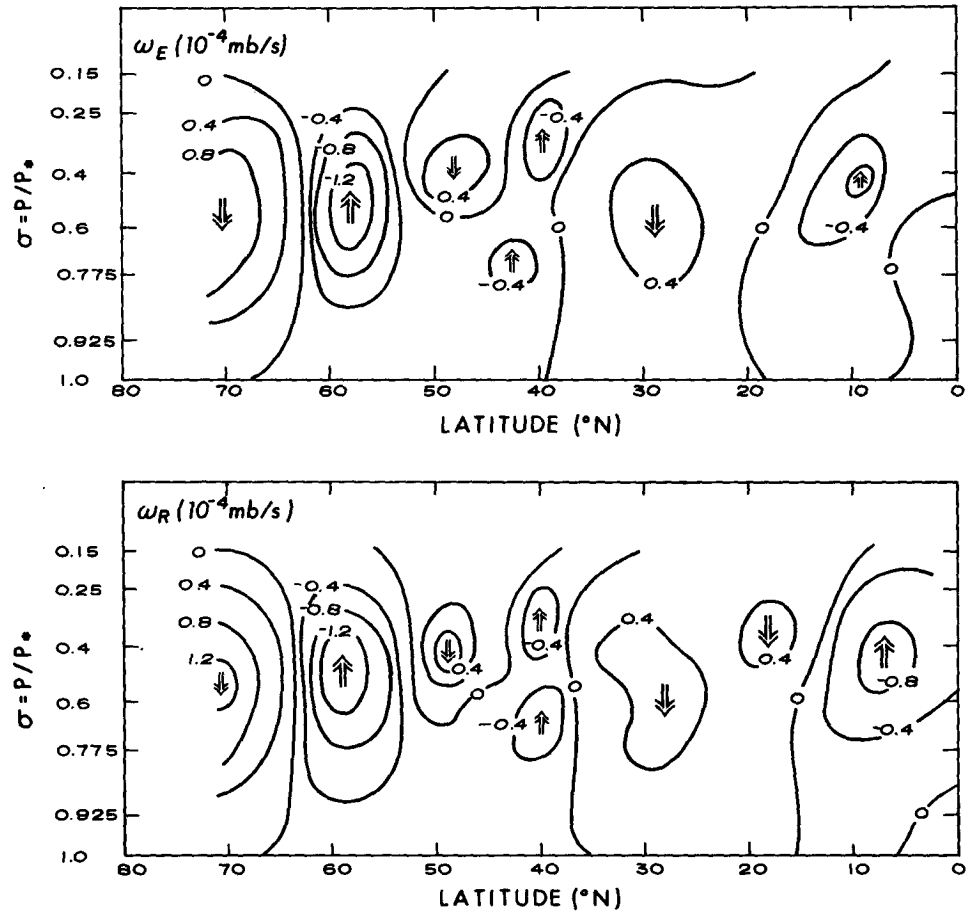

FIG. 22. The predicted, zonally averaged vertical velocity profiles with (lower diagram) and without (upper diagram) the inclusion of the radiative heating–cooling calculation in a GCM on day 5, 11 June 1980. (After Liou and Zheng, 1984.)

predicted vertical velocity zonal profiles at day five with and without the incorporation of the radiative heating–cooling rate calculations, respectively. In reference to the lower diagram, the maximum upward motion is observed at 10°N near about 600 mb, while the downward motion is seen at 30°N. This constitutes the Hadley circulation in the tropical region. There is also a strong maximum upward motion at ~60°N. On both sides of this maximum, downward motions are observed with maxima located at ~50 and 70°N. These patterns constitute the basic meridional circulation in middle latitudes and another Hadley cell in high latitudes. When the radiative heating–cooling processes are removed in the model, there are a number of noticeable modifications to the vertical velocity patterns. The Hadley circulation in the tropical region is significantly weakened in both magnitude and extent. Also, the upward and downward motions located at ~60° and 50°N decrease slightly in magnitude, indicating the possibility of a reduction of intensity in the meridional circulation. As pointed out in their paper, the decreases in the zonal vertical velocities are due to the neglect of radiative cooling rate calculations, which under cloudy conditions would produce significant vertical and horizontal differentials. In turn, these horizontal and vertical inhomogeneities in radiative cooling lead to the intensification of the vertical velocity. We suspect that this dynamic intensification is closely related to the interactions of cirrus clouds and IR radiative flux exchanges in the model. It should be noted that this example is given to induce the potential effects of cirrus cloud–radiation interactions and feedbacks in general circulation models in conjunction with medium range weather prediction. Certainly, this is a research area requiring further numerical experimentation in order to physically sort out the intricate interactions of radiation, clouds and dynamic processes in weather prediction models.

6. Summary

In this review, our current understanding and knowledge of the composition and structure as well as the radiative properties of cirrus clouds have been documented. Moreover, we have also presented the results of numerical experiments derived from models with varying degrees of complexity which reveal some quantitative measures of the influence of cirrus clouds on the temperature structure of the earth–atmosphere system. In view of these discussions and in light of numerous problems presented, it is evident that cirrus clouds are one of the most important, yet least understood atmospheric elements in our weather and climate systems. It is not surprising that cirrus clouds have been singled out as one of the two cloud types (cirrus and stratus) for intensive process experiments (Bretherton and Suomi, 1983). Clearly, in order to construct a reliable numerical model for weather and climate prediction, the dynamic and radiative properties of cirrus clouds must be treated accurately within the context of a model setting.

In his authoritative review describing the importance of cloud modeling in weather and climate studies, Arakawa (1975) pointed out the necessity of establishing a global climatology of the geographical and seasonal distribution of clouds, in which high, middle and low clouds are treated separately so as to verify and "tune" the cloud model developed. He indicated that the cloud cover alone is of very little help in modeling clouds and cloud processes. After reviewing and unifying the subject areas related to cirrus clouds and associated with dynamic and climate processes, it is my physical understanding that the need for a global cloud climatology including cover, height, and some measure of the thickness is particularly pertinent to high cirrus clouds. In the preceding reviews and discussions, I have indicated a number of unsolved research areas which are of experimental and theoretical interest. However, in a global perspective and in the context of weather and climate modeling for the purpose of a physical understanding of the cause and effect relationships and for prediction, it is submitted that the following research programs associated with cirrus clouds are important and therefore should be given the highest consideration:

- It is necessary to have a global cirrus cloud climatology including cloud cover, height and thickness. Presumably, ISCCP (Schiffer and Rossow, 1983), mentioned previously, will provide a comprehensive cloud cover climatology including cirrus clouds. However, the determination of reliable cirrus cloud height and thickness information will require additional efforts. It seems not unlikely that satellite sounding techniques for the retrieval of these cloud parameters could be developed from the currently available imagery and sounding channels. However, they must be verified by the cloud truth data described below. Such information in a limited sense may also be determined by properly setting up a ground-based lidar network. The lidar is particularly useful for the detection of invisible cirrus.
- A number of comprehensive dynamic, cloud and radiation field programs covering several localities and different seasons could be carried out. The FIRE program mentioned above will undoubtedly provide useful information on cirrus clouds. It would be desirable to reduce the uncertainty involved in the cirrus IR emissivity and solar albedo from experimental as well as theoretical sources and to derive the climatological mean and variance of these values in connection with the development and improvement of climate models. Moreover, aircraft observations of solar heating and IR cooling rates in a variety of cirrus cloudy conditions should be performed to cross check and verify the results derived from various theoretical means, and to

assist in the development of parameterization methods for incorporation into numerical models.

• The physical fundamentals and parameterization for the formation of cirrus clouds need to be developed in conjunction with large-scale weather and climate models. In addition, the manner in which the ice content is generated in the model should be connected to the radiative transfer calculations. The aforementioned cloud and cloud radiative data may then be used to verify and tune the cirrus cloud model developed.

Acknowledgments. This research was supported by the Air Force Geophysics Laboratory under Contract F19628-84-K-0040, NASA under Grant NAG5-732 and the Atmospheric Sciences Division, National Science Foundation under Grant ATM-81-09050. I am indebted to a number of my associates and students who provided me with the necessary information for the completion of this review paper. In particular, I thank S. Kinne and A. Peyrefitte for their assistance. S. Bennett typed and edited the manuscript. I also thank G. Paltridge, representing the Radiation Commission of IAMAP, for inviting me to write a review article on the subject of cirrus clouds. Finally, encouragement from H. Bölle and J. Lenoble is appreciated.

REFERENCES

Ackerman, T. P., K. N. Liou and C. B. Leovy, 1976: Infrared radiative transfer in polluted atmospheres. *J. Appl. Meteor.*, **15,** 28–35.

Appleman, H. S., 1961: Occurrence and forecasting of cirrostratus clouds. WMO, 109, Tech. Paper 40, World Meteorological Organization, Geneva, 29 pp.

Arakawa, A., 1975: Modelling clouds and cloud processes for use in climate models. GARP Publ. Ser. No. 16, WMO, 183–197.

Arking, A., and K. Grossman, 1972: The influence of line shape and band structure on temperatures in planetary atmospheres. *J. Atmos. Sci.*, **29,** 937–949.

Asano, A., 1983a: Light scattering by horizontally oriented spheroidal particles. *Appl. Opt.*, **22,** 1390–1396.

——, 1983b: Transfer of solar radiation in optically anisotropic ice clouds. *J. Meteor. Soc. Japan,* **61,** 402–413.

——, and M. Sato, 1980: Light scattering by randomly oriented spheroidal particles. *Appl. Opt.*, **19,** 962–974.

Auer, A. H., Jr., and D. L. Veal, 1970: The dimension of ice crystals in natural clouds. *J. Atmos. Sci.*, **27,** 919–926.

Aufm Kampe, H. J., and H. K. Weickmann, 1957: Physics of clouds. *Meteorological Research Reviews,* Vol. 3, Amer. Meteor. Soc., 182–225.

Barber, P., and C. Yeh, 1975: Scattering of electromagnetic waves by arbitrarily shaped dielectric bodies. *Appl. Opt.*, **14,** 2864–2872.

Barton, I. J., 1983: Upper level cloud climatology from an orbiting satellite. *J. Atmos. Sci.*, **40,** 435–447.

Bretherton, F. P., and V. E. Suomi, 1983: First International Satellite Cloud Climatology Project Regional Experiment (FIRE) Research Plan, 76 pp. [Available from the National Climatic Program Office, Rm. 108, 11400 Rockville Pike, Rockville, MD., 20852.]

Cai, Q. M., and K. N. Liou, 1982: Theory of polarized light scattering by hexagonal ice crystals. *Appl. Opt.*, **21,** 3569–3580.

Chahine, M. T., H. H. Aumann and F. W. Taylor, 1977: Remote sensing of cloudy atmospheres. Part III: Experimental verification. *J. Atmos. Sci.*, **34,** 758–765.

Changnon, S. A., 1981: Midwestern cloud, sunshine and temperature trends since 1901: Possible evidence of jet contrail effects. *J. Appl. Meteor.*, **20,** 496–508.

Charlock, T. P., 1982: Cloud optical feedback and climate stability in a radiative-convective model. *Tellus,* **34,** 245–254.

Chou, M. D., and A. Arking, 1980: Computation of infrared cooling rates in the water vapor bands. *J. Atmos. Sci.*, **37,** 855–867.

——, and ——, 1981: An efficient method for computing the absorption of solar radiation by water vapor. *J. Atmos. Sci.*, **38,** 798–807.

——, L. Peng and A. Arking, 1982: Climate studies with a multilayer energy balance model. Part II: the role of feedback mechanisms in the CO_2 problem. *J. Atmos. Sci.*, **39,** 2657–2666.

Chylek, P., and V. Ramaswamy, 1982: Simple approximation for infrared emissivity of water clouds. *J. Atmos. Sci.*, **39,** 171–177.

Coakley, J. A., and F. P. Bretherton, 1982: Cloud cover from high-resolution scanner data: Detecting and allowing for partially filled fields of view. *J. Geophys. Res.*, **87,** 4917–4932.

Conover, J., 1960: Cirrus patterns and related air motions near the jet stream as derived by photography. *J. Meteor.* **17,** 532–546.

Cox, S. K., 1971: Cirrus clouds and the climate. *J. Atmos. Sci.*, **28,** 1513–1515.

——, 1976: Observations of cloud infrared effective emissivity. *J. Atmos. Sci.*, **33,** 287–289.

Curran, R. J., and M. L. C. Wu, 1982: Skylab near-infrared observations of clouds indicating supercooled liquid water droplets. *J. Atmos. Sci.*, **39,** 635–647.

Derr, V. E., N. L. Abshire, R. E. Cupp and G. T. McNice, 1977: Depolarization of lidar returns from virga and source cloud. *J. Appl. Meteor.* **15,** 1200–1203.

Doswell, C. A., III, and J. T. Schaefer, 1976: Picture of the Month—On the relationship of cirrus clouds to the jet stream. *Mon. Wea. Rev.*, **104,** 105–106.

Drummond, A. J., and J. R. Hickey, 1971: Large-scale reflection and absorption of solar radiation by clouds as influencing earth radiation budget: New aircraft measurement. *Preprints, Int. Conf. on Weather Modification,* Canberra, Aust. Acad. Sci. and Amer. Meteor. Soc., 267–276.

Erickson, C. O., 1974: Picture of the Month—A jet stream cirrus shield. *Mon. Wea. Rev.*, **102,** 260–261.

Feddes, R. G., and K. N. Liou, 1978: Atmospheric ice and water content derived from parameterization of Nimbus 6 high resolution infrared sounder data. *J. Appl. Meteor.*, **17,** 536–551.

Feigelson, E. M., 1981: *Radiation in Cloudy Atmosphere.* Section of Meteorology and Atmospheric Physics of Soviet Geophysical Committees, Hydrometeorology Press (IZD), 280 pp.

Fleming, J. R., and S. K. Cox, 1974: Radiative effects of cirrus clouds. *J. Atmos. Sci.*, **31,** 2182–2188.

Fraedrich, K., E. Ruprecht and V. Trunte, 1976: Determination of the cirrus outflow divergence as seen by satellite. *J. Appl. Meteor.*, **15,** 1312–1316.

Freeman, K. P., and K. N. Liou, 1979: Climatic effects of cirrus clouds. *Advances in Geophysics,* Vol. 21, Academic Press, 231–287.

Greenler, R., 1980: *Rainbows, Halos, and Glories.* Cambridge University Press, 195 pp.

Griffith, K. T., and S. K. Cox, 1977: Infrared radiative properties of tropical cirrus inferred from broadband measurements. Atmos. Sci. Paper No. 269, Colorado State University, 102 pp. [NTIS No. PB-268531]

——, —— and R. G. Knollenberg, 1980: Infrared radiative properties of tropical cirrus clouds inferred from aircraft measurements. *J. Atmos. Sci.*, **37,** 1077–1087.

Hahn, C. J., S. G. Warren, J. London, R. M. Chervin and R. Jenne, 1982: *Atlas of Simultaneous Occurrence of Different Cloud Types over the Ocean.* NCAR/TN-201+STR, National Center for Atmospheric Research, 212 pp.

Harimaya, T., 1968: On the shape of cirrus uncinus clouds: A numerical computation—Studies of cirrus clouds: Part III. *J. Meteor. Soc. Japan,* **46,** 272–279.

Hartmann, D. L., and D. A. Short, 1980: On the use of earth radiation budget statistics for studies of clouds and climate. *J. Atmos. Sci.*, **37,** 1233–1250.

Herman, G. F., M. L. C. Wu and W. T. Johnson, 1980: The effect

of clouds on the earth's solar and infrared radiation budgets. *J. Atmos. Sci.*, **37**, 1251–1261.
Heymsfield, A. J., 1972: Ice crystal terminal velocities. *J. Atmos. Sci.*, **29**, 1348–1356.
——, 1975a: Cirrus uncinus generating cells and the evolution of cirroform clouds. Part I: Aircraft observations of the growth of the ice phase. *J. Atmos. Sci.*, **32**, 798–808.
——, 1975b: Cirrus uncinus generating cells and the evolution of cirroform clouds. Part II: The structure and circulations of the cirrus uncinus generating head. *J. Atmos. Sci.*, **32**, 809–819.
——, 1975c: Cirrus uncinus generating cells and the evolution of cirroform clouds. Part III: Numerical computations of the growth of the ice phase. *J. Atmos. Sci.*, **32**, 820–830.
——, 1977: Precipitation development in stratiform ice clouds: A microphysical and dynamical study. *J. Atmos. Sci.*, **34**, 367–381.
——, and R. G. Knollenberg, 1972: Properties of cirrus generating cells. *J. Atmos. Sci.*, **29**, 1358–1366.
——, and C. M. R. Platt, 1984: A parameterization of the particle size spectrum of ice clouds in terms of the ambient temperature and the ice water content. *J. Atmos. Sci.*, **41**, 846–855.
Hobbs, P. V., L. F. Radke and D. G. Atkinson, 1975: Airborne measurements and observations in cirrus clouds. AFCRL-TR-75-0249, Air Force Geophysics Laboratory, Hanscom AFB, 117 pp.
Irvine, W. M., and J. B. Pollack, 1968: Infrared optical properties of water and ice spheres. *Icarus*, **8**, 324–360.
Jacobowitz, H., 1971: A method for computing transfer of solar radiation through clouds of hexagonal ice crystals. *J. Quant. Spectrosc. Radiat. Transfer*, **11**, 691–695.
Jayaweera, D. O., and B. J. Mason, 1965: The behavior of freely falling cylinders and cones in a viscous fluid. *J. Fluid Mech.*, **22**, 709–720.
Kerker, M., 1969: *The Scattering of Light and Other Electromagnetic Radiation*, Academic Press, 666 pp.
Kessler, E., 969: *On the Distribution and Continuity of Water Substance in Atmospheric Circulation. Meteor. Monog.*, **10**, No. 32, Amer. Meteor. Soc., 84 pp.
Knollenberg, R. G., 1970: The optical array: an alternative to scattering or extinction for airborne particle size determination. *J. Appl. Meteor.*, **9**, 86–103.
Lenoble, J., Ed., 1977: *Standard Procedures to Compute Atmospheric Radiation Transfer in a Scattering Atmosphere.* Radiation Commission, Int. Assoc. of Meteor. and Atmos. Phys., National Center for Atmospheric Research, 125 pp.
Liou, K. N., 1972a: Electromagnetic scattering by arbitrarily oriented ice cylinders. *Appl. Opt.*, **11**, 667–674.
——, 1972b: Light scattering by ice clouds in the visible and infrared: A theoretical study. *J. Atmos. Sci.*, **29**, 524–536.
——, 1973: Transfer of solar irradiance through cirrus cloud layers. *J. Geophys. Res.*, **78**, 1409–1418.
——, 1974: On the radiative properties of cirrus in the window region and their influence on remote sensing of the atmosphere. *J. Atmos. Sci.*, **31**, 522–532.
——, 1976: On the absorption, reflection and transmission of solar radiation in cloudy atmospheres. *J. Atmos. Sci.*, **33**, 789–805.
——, 1977: Remote sensing of the thickness and composition of cirrus clouds from satellites. *J. Appl. Meteor.*, **16**, 91–99.
——, 1980: *An Introduction to Atmospheric Radiation*, Academic Press, 404 pp.
——, and Lahore, 1974: Laser sensing of cloud composition: A backscattered depolarization technique. *J. Appl. Meteor.*, **13**, 257–263.
——, and T. Sasamori, 1975: On the transfer of solar radiation in aerosol atmospheres. *J. Atmos. Sci.*, **36**, 1261–1273.
——, and G. D. Wittman, 1979: Parameterization of the radiative properties of clouds. *J. Atmos. Sci.*, **36**, 1261–1273.
——, and R. F. Coleman, 1980: Light scattering by hexagonal columns and plates. *Light Scattering by Irregularly Shaped Particles*, Plenum, 207–218.
——, and K. L. Gebhart, 1982: Numerical experiments on the thermal equilibrium temperature in cirrus cloudy atmospheres. *J. Meteor. Soc. Japan*, 570–582.
——, and Q. Zheng, 1984: A numerical experiment on the interactions of radiation, clouds and dynamic processes in a general circulation model. *J. Atmos. Sci.*, **41**, 1513–1535.
London, J., 1957: A study of the atmospheric heat balance. Final Rep., Contract AF19(122)-165. Dept. of Meteor. and Oceanogr., New York University, 99 pp. [AST1A 117227, Air Force Geophysics Laboratory, Hanscom AFB, Mass 01730.]
Ludlam, F. H., 1948: The forms of ice clouds. *Quart. J. Roy. Meteor. Soc.*, **74**, 39–56.
——, 1956: The forms of ice clouds, II. *Quart J. Roy. Meteor. Soc.*, **82**, 257–265.
McCleese, D. J., and L. S. Wilson, 1976: Cloud top heights from temperature sounding instruments. *Quart. J. Roy. Meteor. Soc.*, **102**, 781–790.
Machta, L., and T. Carpenter, 1971: Trends in high cloudiness at Denver and Salt Lake City. *Man's Impact on Climate*, W. H. Matthews, W. W. Kellogg and G. D. Robinson, Eds., MIT Press, 410–415.
Manabe, S., 1975: Cloudiness and the radiative convective equilibrium. *The Changing Global Environment*, S. F. Singer, Ed., Reidel, 175–176.
——, and R. F. Strickler, 1964: Thermal equilibrium of the atmosphere with a convective adjustment. *J. Atmos. Sci.*, **21**, 361–385.
——, and R. T. Wetherald, 1980: On the distribution of climate change resulting from an increase in CO_2 content of the atmosphere. *J. Atmos. Sci.*, **37**, 99–118.
Ogura, Y., and T. Takahashi, 1971: Numerical simulation of the life cycle of a thunderstorm cell. *Mon. Wea. Rev.*, **99**, 895–911.
Ohring, G., and P. Clapp, 1980: The effect of changes in cloud amount on the net radiation at the top of the atmosphere. *J. Atmos. Sci.*, **37**, 447–454.
Ono, A., 1969: The shape and riming properties of ice crystals in natural clouds. *J. Atmos. Sci.*, **26**, 138–147.
Ou, S. C. S., and K. N. Liou, 1984: A two-dimensional radiation-turbulence climate model: I. Sensitivity to cirrus radiative properties. *J. Atmos. Sci.*, **41**, 2289–2309.
Pal, S. R., and A. I. Carswell, 1977: The polarization characteristics of lidar scattering from snow and ice crystals in the atmosphere. *J. Appl. Meteor.*, **16**, 70–80.
Paltridge, C. W., and C. M. R. Platt, 1981: Aircraft measurements of solar and infrared radiation and the microphysics of cirrus clouds. *Quart. J. Roy. Meteor. Soc.*, **107**, 367–380.
Peng, L., M. D. Chou and A. Arking, 1982: Climate studies with a multi-layer energy balance model. Part I: Model description and sensitivity to the solar constant. *J. Atmos. Sci.*, **39**, 2639–2656.
Platt, C. M. R., 1973: Lidar and radiometric observations of cirrus clouds. *J. Atmos. Sci.*, **30**, 1191–1204.
——, 1975: Infrared emissivity of cirrus-simultaneous satellite, lidar, and radiometric observations. *Quart. J. Roy. Meteor. Soc.*, **101**, 119–126.
——, and D. J. Gambling, 1971: Emissivity of high layer clouds by combined lidar and radiometric techniques. *Quart. J. Roy. Meteor. Soc.*, **97**, 322–325.
——, and A. C. Dilley, 1981: Remote sounding of high clouds. IV. Observed temperature variations in cirrus optical properties. *J. Atmos. Sci.*, **38**, 1069–1082.
——, N. L. Abshire and G. T. McNice, 1978: Some microphysical properties of an ice cloud from lidar observation of horizontally oriented crystals. *J. Appl. Meteor.*, **17**, 1220–1224.
——, D. W. Reynolds and N. L. Abshire, 1980: Satellite and lidar observations of the albedo, emittance and optical depth of cirrus compared to model calculations. *Mon. Wea. Rev.*, **108**, 195–204.
Potter, G. L., H. W. Ellsaesser, M. C. MacCracken and F. M. Luther, 1978: Atmospheric statistical dynamic models, model performance: The Lawrence Livermore Laboratory zonal atmospheric

model. JOC Study Conf. on Climate Models: Performance, Intercomparison and Sensitivity Studies. Geneva, WMO, Publ. Ser. No. 22, 852–871.

Ramanathan, V., E. J. Pitcher, R. C. Malone and M. L. Blackmon, 1983: The response of a spectral general circulation model to refinements in radiative processes. *J. Atmos. Sci.*, **40,** 605–630.

Reuss, J. H., 1967: Wolken-Stereomessbildreichen, II; Grossraumige cirrus bandes als merkale von Luftmassengrenzen der hohes troposphare and ihrer Eigenshaften. *Beitr. Phys. Atmos.*, **36,** 7–15.

Reynolds, D. W., T. H. Vonder Haar and S. K. Cox, 1975: The effect of solar radiation absorption in the tropical troposphere. *J. Appl. Meteor.*, **14,** 433–443.

Roads, J. O., 1978: Numerical experiments on the sensitivity of an atmospheric hydrologic cycle to the equilibrium temperature. *J. Atmos. Sci.*, **35,** 753–773.

Roewe, D., and K. N. Liou, 1978: Influence of cirrus clouds on the infrared cooling rate in the troposphere and lower stratosphere. *J. Appl. Meteor.*, **17,** 92–106.

Rossow, W. B., E. Kinsella and L. Garder, 1983: Seasonal and global cloud variations deduced from polar orbiting satellite radiance measurements. *Preprints, Fifth Conf. on Atmospheric Radiation,* Baltimore, Amer. Meteor. Soc., 1995–1998.

Sasamori, T., J. London and D. V. Hoyt, 1972: *Radiation budget of the Southern Hemisphere. Meteor. Monogr.*, No. 35, Amer. Meteor. Soc., Chapt. 2.

Sassen, K., 1974: Depolarization of laser light backscattered by artificial clouds. *J. Appl. Meteor.*, **13,** 923–933.

——, 1977: Ice crystal habit discrimination with the optical backscatter depolarization technique. *J. Appl. Meteor.*, **16,** 425–431.

——, and K. N. Liou, 1979a: Scattering of polarized laser light by water droplet, mixed phase, and ice crystal clouds: I. Angular scattering patterns. *J. Atmos. Sci.*, **36,** 838–851.

——, and ——, 1979b: Scattering of polarized laser light by water droplet, mixed phase and ice crystal clouds: II. Angular depolarizing and multiple scattering behavior. *J. Atmos. Sci.*, **36,** 852–861.

Schaaf, J. W., and D. Williams, 1973: Optical constants of ice in the infrared. *J. Opt. Soc. Amer.*, **63,** 726–732.

Schaefer, F. J., 1951: Snow and its relationship to experimental meteorology. *Compendium of Meteorology,* T. F. Malone, Ed., Amer. Meteor. Soc., 221–234.

Schiffer, R. A., and W. R. Rossow, 1983: The international satellite cloud climatology project (ISCCP): The first project of the world climate research programme. *Bull. Amer. Meteor. Soc.*, **64,** 779–784.

Scheider, S. H., W. M. Washington and R. M. Chervin, 1978: Cloudiness as a climate feedback mechanism: Effects on cloud amounts of prescribed global and regional surface temperature changes in the NCAR GCM. *J. Atmos. Sci.*, **35,** 2207–2221.

Smagorinsky, J., 1978: Modeling and predictability. *Studies in Geophysics: Energy and Climate.* Nat. Acad. Sci., Washington, DC, 133–139.

Smith, W. L., and H. M. Woolf, 1976: The use of eigenvectors of statistical covariance matrices for interpreting satellite sounding radiometer observations. *J. Atmos. Sci.*, **33,** 1127–1140.

Spinhirne, J. D., M. Z. Hansen and J. Simpson, 1983: The structure and phase of cloud tops as observed by polarization lidar. *J. Climate Appl. Meteor.*, **22,** 1319–1331.

Starr, D. O., 1984: Radiative modulations of convective elements in cirrus clouds. *Preprints, Fifth Conf. on Atmospheric Radiation,* Baltimore, Amer. Meteor. Soc., 173–176.

Stephens, G. L., 1980a: Radiative properties of cirrus clouds in the infrared region. *J. Atmos. Sci.*, **37,** 435–445.

——, 1980b: Radiative transfer on a linear lattice: Application to anisotropic ice crystal clouds. *J. Atmos. Sci.*, **37,** 2095–2104.

——, 1984: The parameterization of radiation for numerical prediction and climate models. *Mon. Wea. Rev.*, **112,** 826–867.

——, and P. J. Webster, 1981: Clouds and climate: Sensitivity of simple systems. *J. Atmos. Sci.*, **38,** 235–247.

Sundqvist, H., 1978: A parameterization scheme for non-convective condensation including prediction of cloud water content. *Quart. J. Roy. Meteor. Soc.*, **104,** 677–690.

——, 1981: Prediction of stratification clouds: Results from a 5-day forecast with a global model. *Tellus,* **33,** 242–253.

Turner, F. M., and L. F. Radke, 1973: The design and evaluation of an airborne optical ice particle counter. *J. Appl. Meteor.*, **12,** 1309–1318.

Varley, D. J., I. D. Cohen and A. A. Barnes, 1980: Cirrus particle distribution study, Part VII. AFGL-TR-80-0324, Air Force Geophysics Laboratory, Hanscom AFB, 82 pp.

Warren, S. G., 1984: Optical constants of ice from ultraviolet to the microwave. *Appl. Opt.*, **23,** 1206–1225.

Weickmann, H. K., 1945: Formen und Bildung atmosphärisher Eiskristalle. *Beitr. Phys. Atmos.*, **28,** 12–52.

——, 1947: Die Eisphase in der Atmosphäre. Library Trans. 273, Royal Aircraft Establishment, 96 pp.

Wendling, P., R. Wendling and H. K. Weickmann, 1979: Scattering of solar radiation by hexagonal ice crystals. *Appl. Opt.*, **18,** 2663–2671.

Wetherald, R. T., and S. Manabe, 1975: The effects of changing the solar constant on the climate of a general circulation model. *J. Atmos. Sci.*, **32,** 2044–2059.

——, and ——, 1980: Cloud cover and climate sensitivity. *J. Atmos. Sci.*, **37,** 1485–1510.

Wexler, R., and W. C. Skellman, 1979: Picture of the Month–Satellite detection of a long curving cirrus plume. *Mon. Wea. Rev.*, **107,** 343–346.

Wiscombe, W. J., 1980: Improved Mie scattering algorithms. *Appl Opt.*, **19,** 1505–1509.

——, R. M. Welch and W. D. Hall, 1984: The effects of very large drops on cloud adsorption. Part I: Parcel models. *J. Atmos. Sci.*, **41,** 1336–1355.

Woodbury, G. E., and M. P. McCormick, 1983: Global distribution of cirrus clouds determined from SAGE data. *Geophys. Res. Lett.*, **10,** 1180–1183.

——, and ——, 1986: Zonal and geographical distributions of cirrus clouds determined from SAGE data. *J. Geophys. Res.*, **91,** 2775–2785.

Wu, M. L. C., 1984: Radiative properties and emissivity parameterization of high level thin clouds. *J. Climate Appl. Meteor.*, **23,** 1138–1147.

Yagi, T., 1969: On the relation between the shape of cirrus clouds and the static stability of the cloud level. Studies of cirrus clouds: Part IV. *J. Meteor. Soc. Japan,* **47,** 59–64.

——, T. Harimaya and C. Magono, 1968: On the shape and movement of cirrus uncinus clouds by the trigonometric method utilizing stereophotographs—Studies of cirrus clouds: Part I. *J. Meteor. Soc. Japan,* **46,** 266–271.

Yeh, H. Y., 1984: Determination of cloud parameters from infrared sounder data. *J. Geophys. Res.*, **89,** 11759–11770.

——, and K. N. Liou, 1983: Remote sounding of cloud parameters from a combination of infrared and microwave channels. *J. Climate Appl. Meteor.*, **22,** 201–213.